



THE HONG KONG
POLYTECHNIC UNIVERSITY

香港理工大學

Pao Yue-kong Library

包玉剛圖書館

Copyright Undertaking

This thesis is protected by copyright, with all rights reserved.

By reading and using the thesis, the reader understands and agrees to the following terms:

1. The reader will abide by the rules and legal ordinances governing copyright regarding the use of the thesis.
2. The reader will use the thesis for the purpose of research or private study only and not for distribution or further reproduction or any other purpose.
3. The reader agrees to indemnify and hold the University harmless from and against any loss, damage, cost, liability or expenses arising from copyright infringement or unauthorized usage.

IMPORTANT

If you have reasons to believe that any materials in this thesis are deemed not suitable to be distributed in this form, or a copyright owner having difficulty with the material being included in our database, please contact lbsys@polyu.edu.hk providing details. The Library will look into your claim and consider taking remedial action upon receipt of the written requests.

Pao Yue-kong Library, The Hong Kong Polytechnic University, Hung Hom, Kowloon, Hong Kong

<http://www.lib.polyu.edu.hk>

CHANNEL FUNCTION OF CFTR IN BONE CELLS
FOR MICROENVIRONMENT HOMEOSTASIS

ZHANG XIAOTIAN

MPhil

The Hong Kong Polytechnic University

2022

The Hong Kong Polytechnic University

Department of Biomedical Engineering

Channel function of CFTR in bone cells
for microenvironment homeostasis

ZHANG Xiaotian

A thesis submitted in partial fulfilment of the requirements for
the degree of Master of Philosophy

Jun 2021

CERTIFICATE OF ORIGINALITY

I hereby declare that this thesis is my own work and that, to the best of my knowledge and belief, it reproduces no material previously published or written, nor material that has been accepted for the award of any other degree or diploma, except where due acknowledgement has been made in the text.

_____ (Signed)

__ZHANG_Xiaotian_____ (Name of student)

Abstract

The physiological microenvironment for bone cells (e.g., osteocytes and osteoblasts), including the chemical composition, pH and volume of the surrounding interstitial fluid as well as the mechanical forces loaded upon them, is believed to be important for bone cells to function. However, how bone cells interact with these environmental factors remains largely unknown. Cystic fibrosis transmembrane conductance regulator (CFTR) is an anion channel best known for its role in regulating electrolytes and water transport in epithelial tissues. Studies have also demonstrated the channel function of CFTR to be mechanosensitive. Given the reported expression of CFTR in bone cells and the correlation of CFTR mutation with bone defects, we hypothesized that CFTR might play a role in regulating the bone cell microenvironment via its channel functions.

Using patch-clamp analysis in MLO-Y4 cells, a mouse osteocyte-like cell line, whole-currents promoted by forskolin (a cAMP activator) and blocked by CFTR_{inh}-172 (a CFTR selective inhibitor) were observed, suggesting CFTR channel function in bone cells. Fluorometric imaging measurement of intracellular Cl⁻ concentration ([Cl⁻]_i) and membrane potential (V_m) in MLO-Y4 cells showed that CFTR inhibitors induced increases in [Cl⁻]_i and V_m, suggesting CFTR in mediating Cl⁻ efflux in bone cells. Further studies using siRNA-based knockdown and CRISPR-Cas9-based knockout of CFTR in MLO-Y4 cells confirmed CFTR channel function mediating Cl⁻ efflux in bone cells. In addition, fluorometric pH dye monitoring intracellular pH of MLO-Y4 cells showed that CFTR_{inh}-172 impeded pH change recovery from alkalization induced by the removal of extracellular CO₂/HCO₃⁻, suggesting the role of CFTR in mediating the exclusion of HCO₃⁻ and thus in regulating extracellular pH in bone cells. Consistent with this, we found in RNA sequencing analysis of bone tissues from CFTR mutant (DF508) mice that key genes encoding V-ATPase, a

proton pump critically involved in pH regulation, were significantly upregulated in DF508 bones as compared to the wild type. To demonstrate possible mechano-sensitivity of CFTR in bone cells, we used both ultrasound stimulation and stretching forces. Ultrasound elicited intracellular Ca^{2+} elevation and $[\text{Cl}^-]_i$ responses which were largely inhibited by CFTR_{inh}-172. Stretching of MLOY4 cells upregulated COX-2, a key osteogenic gene, which was also inhibited by CFTR_{inh}-172. These results suggested a possible role of CFTR in mediating mechanical stimulation in bone cells. We also tested a mouse osteoblast cell line, MC3T3, which showed similar function of CFTR as Cl^- channel.

Together, these results have demonstrated previously undefined $\text{Cl}^-/\text{HCO}_3^-$ channel function of CFTR in bone cells and suggested its regulatory roles in maintaining the homeostasis of the microenvironment such as mediating electrolyte/water transport, adjusting pH and responding to mechanical stimulation.

Acknowledgement

Although the thesis of my MPhil study takes less than two years to pace here, the pandemic of Covid-19 makes everything seem to have passed for a very long time. I would express my sincere gratitude to the people who support me through these tough times.

Firstly, I felt fortunate to be supervised by Dr. Ruan Yechun, not only for her rigorous and careful guidance for my projects alongside the thesis, but also for her empathetic consideration throughout my tough times. The profound and insightful suggestion provided by Dr. Ruan gives me a good example of performing well in academia. During the pandemic period, she coordinated with other people trying to support my study not to be postponed. In daily life, she is a considerate and patient person. To relieve my pressure, she often talked to me or invited me to participate in the sharing talk hosted by her friends of the church. It opens my horizon to life and teaches me the further meaning of life.

I also appreciate Mr. Hu Peijie for his help and support during my study. Peijie is a hardworking and rigorous person. He is always glad to give suggestions to my experiment. Without his strict check, I could not complete my thesis. Besides, he is also a perseverant person concentrating to research. Although it was challenging to establish the CFTR-knockout MLO-Y4 cells model, he did not give up and successfully established the cell model. Besides, Peijie also contributed to prepare the animal samples for RNA-seq. Without his contribution, I can't complete my study.

I would also express my great gratitude to Dr. Xu Jiankun. He is the first people taught me methodologies for cellular and molecular experiments. With a careful and considerate attitude, he taught me how to do experiments step by step without reservation. Although he is very busy, he is

still patient and glad to answer my naïve questions. As the first research scientist I have met, he is a great model for being a good researcher. His hardworking and modesty touched me deeply, and he has always been my goal of learning.

I will also extend my gratitude to people who support me and give me suggestions. I would thank Dr. Guo Jinghui, Dr. Chen Junjiang, Dr. Chen Hui, Dr. YU Mei Kuen for their sincere help and kind advice. I would also thank Mr. Wu Yong, Ms. Ma Xiyang, Ms. Que Yanting for their membership and support.

Table of contents

Abstract.....	4
Acknowledgement	6
Table of contents.....	8
Abbreviations.....	10
Chapter 1. Introduction	11
1.1. Hierarchical structures of bone.....	11
1.2. Microenvironment in lacunar-canalicular porosity	13
1.3 Functions of lacunar-canalicular microenvironment homeostasis	14
1.4 Cellular regulation of lacunar-canalicular microenvironment homeostasis.....	16
1.5 CFTR	21
1.5.1 CFTR in regulation of fluid homeostasis in epithelial tissues	23
1.5.2 CFTR and bone health	24
1.6 Hypothesis and aim	25
Chapter 2. Methodology	27
2.1 Cell culture.....	27
2.2 CFTR knockdown.....	27
2.3 CFTR knockout by CRISPR-Cas9	28
2.4 RNA extraction and quantitative PCR	29
2.5 RNA sequencing.....	30
2.6 Patch-clamp recording.....	31
2.7 Membrane potential measurement	32
2.8 Intracellular calcium measurement	33
2.9 Intracellular chloride measurement.....	33
2.10 Ultrasound stimulation for gene expression analysis	34
2.11 Ultrasound stimulation for intracellular ions measurement	34
2.12 Statistics.....	34
Chapter 3. Results	35

3.1 CFTR mediates Cl ⁻ efflux in MLO-Y4 cells	35
3.1.1 Channel function of CFTR conducting Cl ⁻	35
3.1.2 Effect of the CFTR inhibitor on intracellular Cl ⁻ concentration and membrane potential	37
3.1.3 Effect of CFTR knockout and knockdown on CFTR conducting Cl ⁻	41
3.1.4 Summary	44
3.2 CFTR contributes to pH regulation in osteocytes	46
3.2.1 Effect of the CFTR inhibitor on HCO ₃ ⁻ secretion and pH maintenance in MLO-Y4 cells.	46
3.2.2 Effect of CFTR knockout on HCO ₃ ⁻ secretion and pH maintenance in MLO-Y4 cells.	48
3.2.3 Involvement of CFTR in pH recovery from intracellular acidification in osteocytes ..	50
3.2.3 Summary	51
3.3 Involvement of CFTR in mechanotransduction in MLO-Y4 cells.....	52
3.3.1 CFTR involved in ultrasound-induced gene expressions in MLO-Y4 cells.....	52
3.3.2 Effects of the CFTR inhibitor on ultrasound-induced change of intracellular Ca ²⁺ and Cl ⁻ concentrations in MLO-Y4 cells.	53
3.3.3 Effects of CFTR inhibitors on stretch-induced gene expressions in MLO-Y4 cells ...	57
3.3.4 Summary	58
3.4 Comparison of CFTR channel functions between MLO-Y4 cells and MC3T3 cells	59
3.4.1 Effect of the CFTR inhibitor on intracellular Cl ⁻ concentration and membrane potential in MLO-Y4 cells and MC3T3 cells	59
3.4.2 pH maintenance in MC3T3 cells.	60
3.4.3 Summary	61
Chapter 4. Discussion	62
4.1 Cl ⁻ in the microenvironment for bone cells.	62
4.2 pH of the microenvironment for bone cells.....	63
4.3 Environmental cues for bone cells.	64
4.4 Conclusion remarks.....	65
References.....	67

Abbreviations

BECF	Bone Extracellular Fluid
cDNA	complementary DNA
CF	Cystic Fibrosis
CFBD	Cystic fibrosis-related bone disease
CFTR	Cystic fibrosis transmembrane conductance regulator
CRISPR	clustered regularly interspaced short palindromic repeats
Δ F508	Deletion of phenylalanine on position 508
DMSO	Dimethyl sulfoxide
ECF	Extracellular Fluid
FBS	Fetal bovine serum
FPKM	Fragments Per Kilobase of transcript per Million mapped reads
LIPUS	Low intensity pulsed ultrasound
mRNA	messenger RNA
NMDG	N-methyl-D-glucamine
PBS	Phosphate-Buffered Saline
PEG2	Prostaglandin E2
qPCR	quantitative Polymerase Chain Reaction
RANKL	Receptor activator of nuclear factor kappa-B ligand
RNA-Seq	RNA sequencing
siRNA	Small interfering RNA
α MEM	Minimum Essential Medium Eagle Alpha

Chapter 1. Introduction

1.1. Hierarchical structures of bone

Integrated by inorganic and organic components, the bone provides mechanical, chemical, and biological functions for our body (Rho, Kuhn-Spearing, Zioupos, & physics, 1998). Functions as a skeleton, the bone demonstrates complex mechanical properties realized by hierarchical microstructures associated with cortical and trabecular bone (Rho et al., 1998). With larger density and less porosity, the cortical bone characterizes the harder part outlining the layer of bone marrow while the trabecular bone consists by honeycomb-like microstructure interacting with bone marrow shown in Figure 1.1.1 (Malhan et al., 2018).

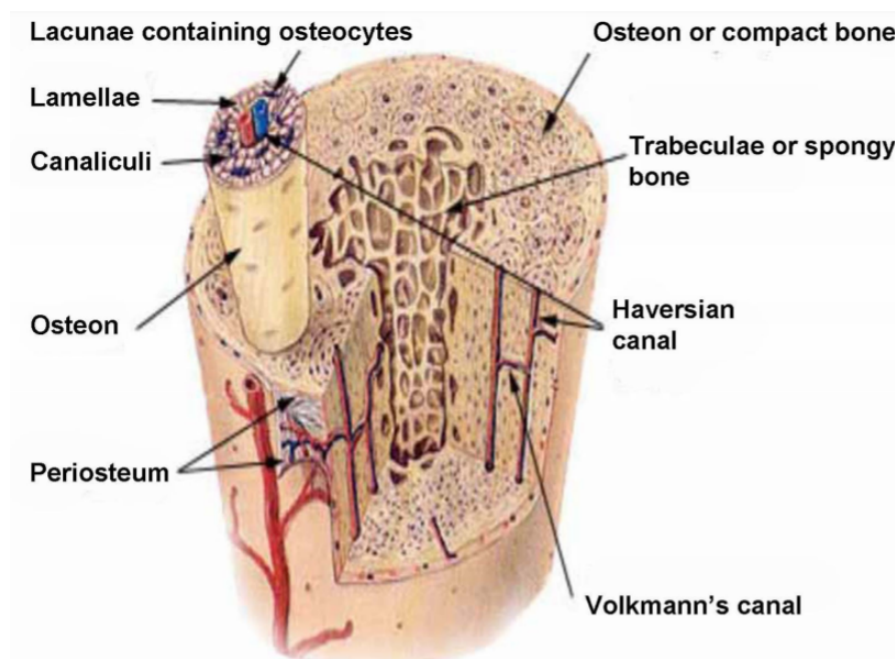


Figure 1.1.1 Hierarchical structures of bone. From “Blood and Interstitial flow in the hierarchical pore space architecture of bone tissue,” by S.C. Cowin and L. Cardoso, 2015, *Journal of biomechanics*, 48(5), 842-854. Copyright © 2014 Elsevier Ltd.

In cortical bones, the cylinder sub microstructure osteon (200–250 μm in diameter) is a functional unit which is also named as the Haversian system shown in Figure 1.1.1. In the central cavity of the Haversian system, lymphatics, arterial and venous vessels and nervous fibers are vertically embraced by concentric collagen lamella. Such longitudinal Haversian canals are interconnected by transverse canals (Volkmann canal, ($\sim 50 \mu\text{m}$ in diameter), which are highly vascularized (Cvetkovic et al., 2013). Inside the vascular porosities shown in Figure 1.1.2 (Albert et al., 2008), another porosity system with smaller size named as lacunar-canalicular systems (LCS) comprised by lacuna cavity (5–10 μm in width) and canaliculi (100–600 nm in diameter) penetrate the concentric layer of lamella. Osteocytes are housed in lacuna with dendritic processes located along canaliculi to form intercellular network (Yu, Pacureanu, Olivier, Cloetens, & Peyrin, 2020).

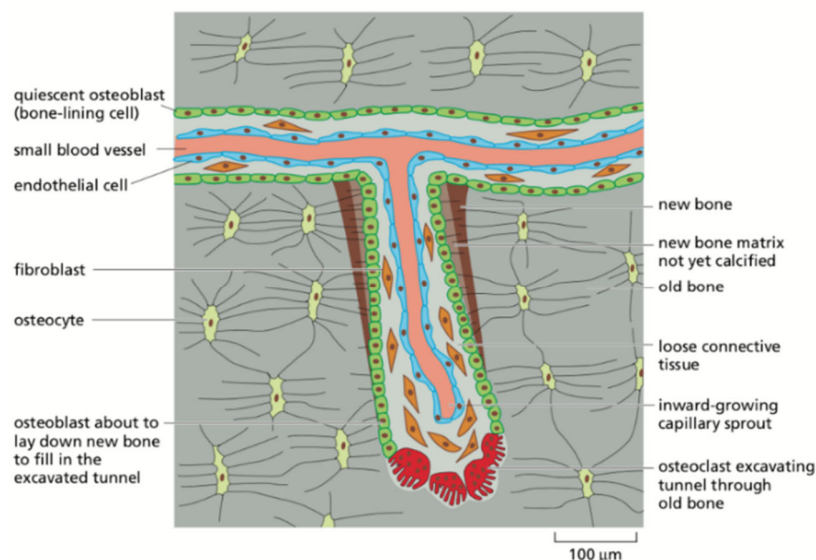


Figure 1.1.2. Blood vessel within bone matrix. Adapted from *Molecular Biology of the Cell* p1473, by B.A. Alberts et al., 2008, Garland Science. Copyright © 2008 by Alberts et al.

1.2. Microenvironment in lacunar-canalicular porosity

There are two types of fluid respectively flowing in vascular porosities and lacunar-canalicular porosities in the bone. Originated from blood and lymphatic streams, a layer of interstitial fluid, named as extracellular fluid (ECF), fills in vascular canals of bone. Quiescent osteoblasts lining the bone surface (i.e. bone lining cells) compartmentalizes ECF from lacunar-canalicular system to form a stable microenvironment for osteocytes. Osteocytes constitute over 95% of all bone cells and play a central role in bone remodeling (Rocheffort, Pallu, & Benhamou, 2010). Embedded in the bone matrix, they are interconnected with each other through their dendritic processes, forming a cellular system called osteocyte lacuno-canalicular system (OLCS) as shown in Figure 1.2 (Bozal, Sánchez, & Ubios, 2012; Buenzli & Sims, 2015).

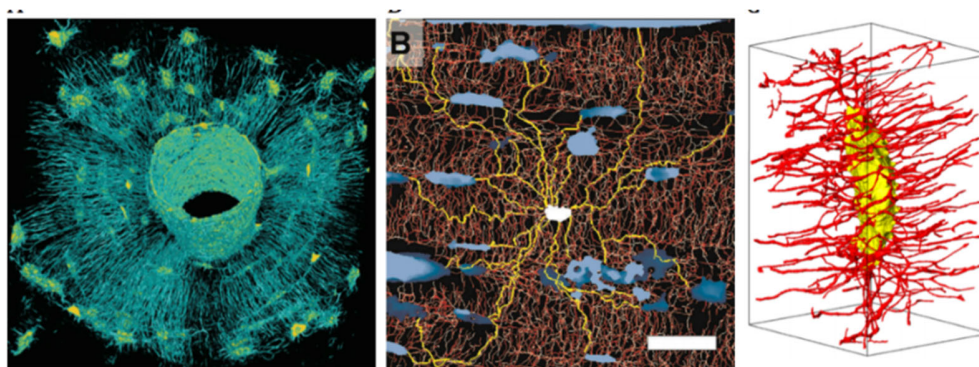


Figure 1.2. Lacunar-canalicular network. Adapted from “Quantifying the osteocyte network in the human skeleton,” by P.B. & N. S. Buenzli and Sims, 2015, *Bone*, 75, 144-150. Copyright © 2015 by Elsevier Inc.

Due to the specialized structure, functions and viability of osteocytes are highly dependent on their surrounding microenvironment. As the dominate factor for the microenvironment, fluid filling in the very thin gap/capacity between osteocytes and surrounding bone matrix is called bone extracellular fluid (BECF). It plays an essential role in the exchange of electrolytes/water,

metabolites, signalling molecules between osteocytes and the ECF which confluent to the blood and lymphatic streams. For these crucial functions, the homeostasis of BECF including electrolytes, pH, biochemical molecules and mechanical force carried by this fluid should be rigorously controlled. It is believed that driven by hydrostatic pressure and mechanical loading, BECF continuously travels through lacunar-canalicular networks and eventually drained into the lymphatic system (Cowin & Cardoso, 2015). It means, originally derived from blood, the homeostasis of BECF should be similar as ECF. However, evidence from the different ionic components in BECF and ECF summarized in Table 1 (Armstrong, Singer, & Research®, 1965), suggesting active roles of bone lining cells and osteocytes in regulating the homeostasis of microenvironment in lacunar-canalicular porosity.

Table 1. Ionic components within ECF and BECF

Mineral content	ECF (mM/L)	BECF (mM/L)
Ca	1.5	0.5
Mg	0.7	0.4
K	4	25
Na	140	125
Pi	1.8	1.8
Cl	100	130

1.3 Functions of lacunar-canalicular microenvironment homeostasis

Housed in the lacuna-canalicular cavities, osteocytes closely interact with the microenvironment in which mainly controlled by the homeostasis of BECF. A number of

physiological functions of BECF are proposed. First, BECF plays an essential role in the bone's biochemical homeostasis (e.g., pH, hormones). In response to the parathyroid hormone, the bone extracellular fluid can function as an exchangeable ionic pool regulating the inward and outward calcium fluxes to maintain the plasma calcium without bone remodeling (Marenzana, Shipley, Squitiero, Kunkel, & Rubinacci, 2005). Disorders of this ion exchange may lead to hypocalcemia (Kovacs, 2014). Decreased pH due to systemic acidosis may initiate the release of alkaline bone mineral in the bone extracellular fluid to maintain the acid-base balance (Arnett, 2003). Such chaotic pH can lead to significant osteoporosis and osteomalacia associated with hypercalcemia (Arnett, 2003).

In addition, it was recently recognized that osteocytes are subject to shear stress from the flow of BECF. (Alessandro Rubinacci et al., 2002). The bone is an electrically dynamic organ with short-lived voltage induced by the mechanical load, and studies have suggested the involvement of such electrical phenomena in the bone mechanotransduction (Borgens, 1984). As the fluid flow with different ionic components and electrolytes, load-induced flowing BECF can generate both shear stress and a streaming potential at the surface of the cell body and dendritic processes along lacuno-canalicular cavities of osteocytes (Dallas, Prideaux, & Bonewald, 2013). The load-induced streaming potential of BECF has been suggested to be responsible for the measured short-lived voltage, enabling the bone to repair and regenerate itself (Huang & Ogawa, 2010). Based on the identification of load-induced streaming potential, pulsed electromagnetic fields have been clinically used as a treatment to enhance fracture healing (Riddle & Donahue, 2009). As another therapeutic strategy to apply mechanical stimulation, low-intensity pulsed ultrasound (LIPUS) has demonstrated positive effects in accelerating bone regeneration (Busse, Bhandari, Kulkarni, & Tunks, 2002). Systematic reviews and meta-analysis of the effects of

LIPUS supported its benefits in accelerating bone fracture healing in both adult and elderly patients (Lou, Lv, Li, Zhang, & Tang, 2017). Characterized by the scaled intensity (30mW/cm²) and frequency (1.5 MHz), LIPUS can induce biological responses of cells including osteoblasts and osteocytes involved in bone-fracture healing with limited thermal effects (Leighton et al., 2017).

1.4 Cellular regulation of lacunar-canalicular microenvironment homeostasis

If the regular functions of osteocytes highly depend on the BECF, there should be an intrinsic mechanism underlying the regulation of the homeostasis of BECF. With the identification of a functional syncytium constituted by bone lining cells and osteocytes, the cellular regulation of the BECF has been gradually revealed. Osteoblasts, in particular, a pool of quiescent osteoblasts (with the flat and fibroblast-like shape) called bone lining cells that connect via gap junctions and cover the inactive (non-remodeling) bone surface (Florencio-Silva, Sasso, Sasso-Cerri, Simões, & Cerri, 2015; Miller, Bowman, & Jee, 1989). Some bone lining cells form gap junctions with osteocytes in lacuno-canalicular cavities through extended processes to form the osteocyte-bone lining cells system (OBLCS) (Aarden, Nijweide, & Burger, 1994). Bone lining cells modulate over the bone surface as the functional compartmentalization maintains ionic components in bone extracellular fluid, which can explain the differentiated ionic components between ECF and ECF summarized in Table 1.

As shown in Figure 1.4.1, aiming to support the BECF regulation with a cellular origin, several methods including Vibrating electrode probe and Scanning ion-selective electrode technique (SIET) have been applied to conduct the *ex vivo* two- and three-dimensional measurements of local ionic gradients on a damaged point of living metatarsal bone samples immersed in bathing solution, which mimics the systemic extracellular fluid (ECF) derived from blood plasma

(Marenzana et al., 2005; A Rubinacci et al., 1998). The purposes for the selected metatarsal bone samples from mice or frogs are mainly due to their avascular structure and less damage on the tissue surface of ensheathments for the intact bone membrane structure (Borgens, 1984; Alessandro Rubinacci, Benelli, Borgo, & Villa, 2000). With alternative ionic components of ECF, different concentration gradients of both cation and anion, including sodium, potassium, calcium as well as bicarbonate and chloride are observed (Alessandro Rubinacci et al., 2002). However, such observation disappears in the dead bone samples, which further suggests that such ionic gradients between ECF and BECF may be regulated by a cellular pump-leak mechanism (Bushinsky, Chabala, Levi-Setti, & Metabolism, 1989). Besides, the measurable transepithelial resistance (110-180 $\Omega\cdot\text{cm}^2$) of a monolayer formed by primary osteoblasts and the observation of claudins and other tight-junction associated proteins in osteoblasts indicate the presence of an epithelial-like ion transport system in bone lining cells (Wongdee et al., 2008), which support the existence of the putative bone membrane.

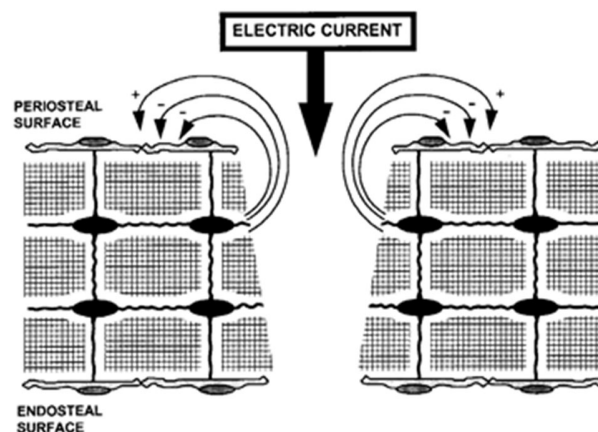


Figure 1.4.1 Schematic illustration for the net current measured by vibrating electrode probe. Adapted from “Osteocyte-bone lining cell system at the origin of steady ionic current in damaged amphibian bone,” by A.R. Rubinacci, 1998, *Calcified tissue international*, 63(4), 331-339. Copyright © 1998 by Springer Nature.

As another part of the OBLCS, osteocytes also demonstrate an essential role in modulating the BECF as their functions are highly correlated to BECF and have enormous contact area for the surrounding fluid. Based on recent studies, osteocytes mainly regulate BECF from mechanotransductive and metabolic aspects. With the application of mechanical loads with modulated amplitudes and frequencies, a dosage-dependent ionic current has been observed in the mice local damaged living metatarsal bone samples measured by the vibrating electrode probe (Alessandro Rubinacci et al., 2002). As shown in Figure 1.4.2, this loads-induced current decays exponentially after the exerted loading (Alessandro Rubinacci et al., 2002). Interestingly, this loads-induced modification of currents is lost by static loads (0 Hz), further suggesting the mechano-sensitive modulation of such current (Alessandro Rubinacci et al., 2002). To explain the cellular modulation of BECF, Rubinacci, in this experiment, proposed a model of an ionic flux model with involvements of stretch-activated ion channels which was shown in Figure 1.4.3. Although this experiment did not directly clarify the role of osteocytes in the modulation of BECF, the load-dependent modulation pattern and intrinsic large contact area of osteocytes for BECF still implied the possible regulation of osteocytes during this process with the involvement of ion channels.

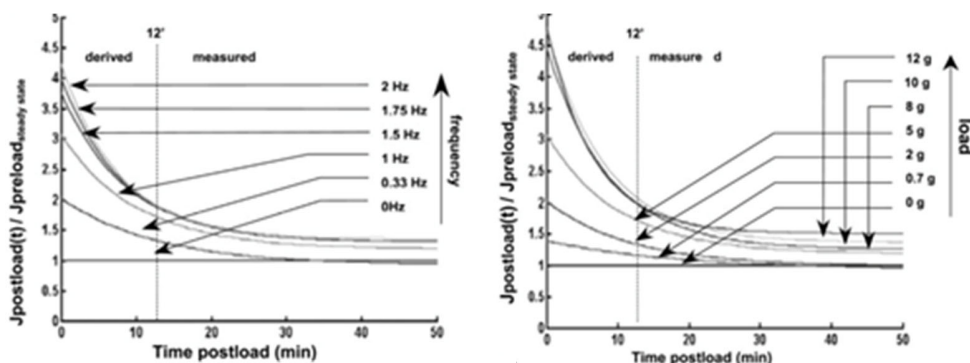


Figure 1.4.2 Single exponential interpolations of current density induced by cyclic loads with different amplitudes and frequencies. Adapted from “Bone as an ion exchange system: evidence for a link between mechanotransduction and metabolic needs,” A.R. Rubinacci et al., 2002, *American Journal of Physiology-Endocrinology And Metabolism*, 282(4), E851-E864. Copyright © 2002 by the American Physiological Society

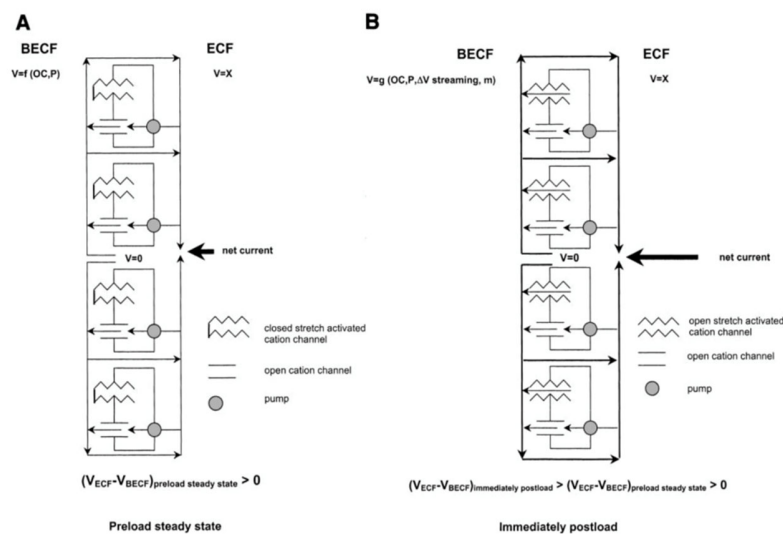


Figure 1.4.3 Model of ionic flux at BECF-ECF interface. Adapted from “Bone as an ion exchange system: evidence for a link between mechanotransduction and metabolic needs,” A.R. Rubinacci et al., 2002, *American Journal of Physiology-Endocrinology And Metabolism*, 282(4), E851-E864. Copyright © 2002 by the American Physiological Society

For the metabolic-needs-induced regulation of BECF, osteocytes recently are suggested to involve in the osteocytic osteolysis for calcium homeostasis. Osteocytic osteolysis is a concept raised over 100 years ago, which describes the observation that osteocyte can remove the surrounding matrix. However, with the identification of osteoclasts, specified bone-resorbing cells

derived from monocytes in bone marrow, the idea of osteocytic osteolysis fell out in the late 1970s (Wysolmerski, 2012). Despite osteoclasts demineralized bone matrix via a proton pump induced acidification, osteocytes have been proposed to dominate in the reversible perilacunar/canalicular remodeling during lactation with similar molecular mechanisms as osteoclasts (Jähn, Kelkar, Zhao, Xie, Tiede-Lewis, Dusevich, Dallas, Bonewald, et al., 2017). In response to parathyroid hormone-related protein (PTHrP), osteocytes can acidify the bone extracellular fluid through secreting protons by the vacuolar proton pump (V-ATPase), a highly conserved evolutionarily protons pump (Jähn, Kelkar, Zhao, Xie, Tiede-Lewis, Dusevich, Dallas, Bonewald, et al., 2017). The acidified fluid removes the perilacunar/pericanalicular matrices to increase calcium in the BECF in which there is a requirement of calcium release. Such increased calcium will be pumped out by the bone lining cells into the ECF, subsequently, join the circulation of blood plasma (Fig. 1.4.4). Besides, osteocytes tend to have higher viability than osteoblasts and fibroblasts at pH as low as 5 *in vitro*, which further suggests the role of osteocyte in pH regulation of the bone extracellular fluid (Jähn, Kelkar, Zhao, Xie, Tiede-Lewis, Dusevich, Dallas, Bonewald, et al., 2017). This osteocyte-dependent acidification may also explain the observation of instantaneous calcium efflux in bone for regulating plasma calcium without bone remodelling (Marenzana et al., 2005). Although osteocytes can demonstrate perilacunar/pericanalicular remodeling through modulating pH of the BECF during lactation, whether this mechanism can be extended to other osteocytic osteolysis observations in response to the physiological stimulus, like parathyroid hormone, calcium restriction, hibernation, and reproductive cycles still unclear.

Despite these previous studies, the exact molecular mechanisms underlying the cellular regulation of bone extracellular fluid remains unclear.

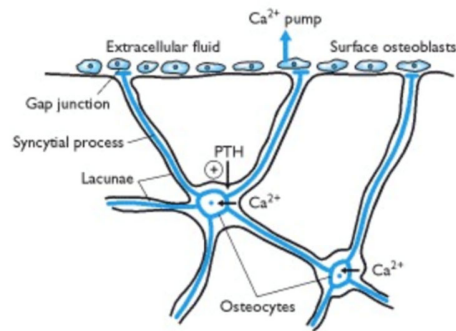


Figure 1.4.4. Schematic illustration for the Ca²⁺ flux through BECF-ECF interface in response to PTH. Adapted from flipper, by E.L. Lerro, 2007, <http://flipper.diff.org/app/items/info/350>.

1.5 CFTR

Cystic Fibrosis Transmembrane Conductance Regulator (CFTR) is a selective anion channel categorized in ATP-binding cassette transporters (ABC transporters) superfamily and extensively expressed in diverse epithelial cells/tissues. The original name of CFTR defined as the autosomal recessive disease cystic fibrosis (CF) is one of the most common genetic diseases with high mortality in Caucasians. As an ion channel in the family of ABC transporters, protein kinase A (PKA)-dependent phosphorylation is mandatory for CFTR activation. Due to this point, cyclic adenosine monophosphate (cAMP) as the activator of PKA makes CFTR also named as “cAMP-activated channel” (Moran & Sciences, 2017). Including the biochemical gating mechanism, researchers have reported that CFTR is mechanosensitive and can be gated by the mechanical stretch (Zhang et al., 2010).

Although cystic fibrosis is a disease with high mortality, improved medical conditions continuously extended life expectancy of patients. A number of associated complications of cystic fibrosis were reported. As a significant complication closely associated with healthy quality of cystic fibrosis patients, cystic fibrosis bone diseases (CFBD) raised attentions from researchers. Recently, CFTR was speculated to not only accompany but directly associate to bone health (Javier & Jacquot, 2011). As the supporting evidence, expression of CFTR has been verified in osteocytes and osteoblasts for both human and mice (Bronckers et al., 2010; Shead et al., 2007; Stalvey et al., 2013). Besides, evidence from our lab in CFTR-deficiency model ($\Delta F508$ mice) also indicated the direct role of CFTR in osteocytes. Assessed by the powerful imaging method SEM, the abnormal morphology about osteocytes could be observed CFTR-deficiency model ($\Delta F508$ mice) (Fig. 1.5)

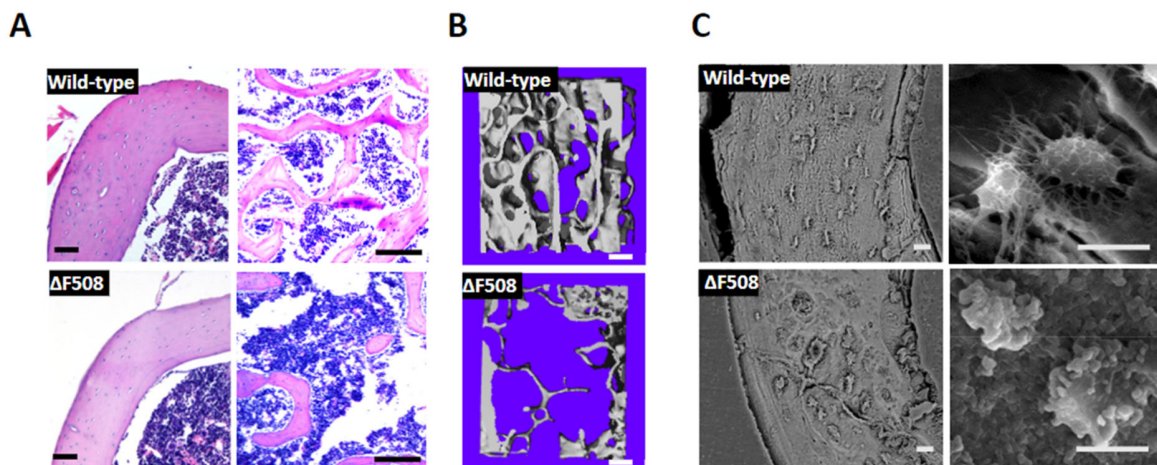


Figure 1.5. (A) Hematoxylin and Eosin staining, (B) micro-CT and (B) scanning electron microscopy images of femoral tissues from $\Delta F508$ and age-matched wild-type mice. Unpublished data from Dr. Sharon Run's Group

1.5.1 CFTR in regulation of fluid homeostasis in epithelial tissues

As the dominated Cl^- channel involved in the transcellular salt secretion process, CFTR regulates the Cl^- exit in the airway surface. CFTR is also permeable to HCO_3^- with less five times conductance than Cl^- . In the epithelia of the airway, the CFTR-dependent secretion of HCO_3^- is involved in pH regulation of the airway surface liquid (Coakley et al., 2003). By modulating the fluidic pH, the CFTR-mediated HCO_3^- participated in the mucus gel formation in the airway through complexing with Ca^{2+} and H^+ , which further indicated the vital role of CFTR in the regulation of the extracellular milieu (Perez-Vilar, Olsen, Chua, & Boucher, 2005).

Functioning as a $\text{Cl}^-/\text{HCO}_3^-$ channel, CFTR is crucial for electrolyte and fluid transport. Different from the polarized expression pattern in the airway, CFTR is present on both apical and basolateral membranes of duct cells in the sweat gland (Quinton, 2007). In the sweat duct, the epithelial sodium channel on the apical membrane and Na^+/K^+ -ATPase across the basolateral membrane can generate the transcellular Na^+ current, which forms the electrochemical gradient favoring Cl^- movement (Saint-Criq & Gray, 2017). Driven by this gradient, Cl^- can be absorbed by apical CFTR and extruded by basolateral CFTR as the lack of intrinsic paracellular permeability of Cl^- (Reddy & Quinton, 1989). Through this mechanism, the absorption of the electrolyte NaCl was regulated by CFTR in the sweat gland. For the involvement of CFTR in fluid transport, it was a tissue-dependent process due to the different permeability of water among different epithelial tissues. In the airway surface, the CFTR-dominated Cl^- net current can drive Na^+ exit, which forms the osmotic pressure to drive the concurrent water paracellularly producing the isotonic fluid. Different from the airway, the sweat gland duct has low water permeability. As a result, this net NaCl absorption due to CFTR in the duct cells will not trigger concurrent water fluid, which finally causes the hypotonic fluid (Quinton, 2007).

CFTR can also regulate other transporters via protein-protein interaction (Guggino & Stanton, 2006). CFTR has been proposed to be necessary for modulating localization and function of V-ATPase in intestinal cells for pH regulation (A. Collaco, Geibel, Geibel, & Ameen, 2011). Moreover, the role of CFTR has been proved to be involved in the organization and function of both the gap and tight junction proteins, which suggested the indirect role of CFTR in paracellular transport through gap and tight junctions (Castellani et al., 2012).

1.5.2 CFTR and bone health

Interestingly, emerging evidence has also suggested the potential role of CFTR in bone health. For the past three decades, with the promotion of medical conditions, emerging complications in CF patients with expanded life span indicated potential involvements of CFTR in not only epithelial tissues and cells but also other types of cells (Aris, Merkel, & Bachrach, 2005). Among these complications, significant bone loss and increased fracture rate in CF patients have been characterized as the phenotype of Cystic fibrosis-related bone disease (CFBD) (Aris et al., 2005). Although CFTR deficiency is associated with some systematic complications such as lung inflammation and intestinal malabsorption which are highly involved in the pathophysiological mechanisms behind CFBD, observation of lower bone mineral density in young CF children aged below 6 years old without influences of nutritional status or disease severity compared to healthy controls suggested the possible direct role of defective CFTR protein for the pathophysiological mechanism in diminished bone development (Javier & Jacquot, 2011). Moreover, mice with F508D-CFTR genotype, which was the most common mutation of CFTR, demonstrated the significantly decreased bone formation and bone loss (Le Henaff et al., 2015). Therefore, these experiments and clinical manifestations have indicated a direct role of CFTR in bone health.

However, the exact role of CFTR in bone physiology remains unclear. Although scientists focused more on osteoblasts at regenerative level of bone tissues due to the bone remodeling process, more and more attractions had been drawn to osteocytes. As the terminated status of bone cells, osteocytes have the largest number and longer life in bone tissues with amazing function to form a cellular network orchestrating other bone cell. Based on their specific anatomy structure, the only way for osteocytes to exchange substance and signals with circulation systems is surrounding microenvironment. Also, their dendritic probing contact with surrounding space offer them the largest contact areas with bone matrix among all other bone cells. Inspired by this unique structure-based function, we speculated that CFTR, which was generally involved in fluidic regulation in epithelial tissues, might contribute to some physiological process in osteocytes to fulfill their multifunction.

1.6 Hypothesis and aim

The lacunar-canalicular microenvironment is essential for providing nutrition, exchanging materials, and transducing mechanical load for osteocytes living in bone compartmentalization. To achieve these purposes, the homeostasis (Chemical, Biological and Mechanical elements) of the microenvironment is realized by the fluid BECF. As the exchangeable pool with electrolytes, hormones and pH, the bone extracellular fluid interacts with osteocytes as well as osteoblasts to participate in mineral homeostasis and acid-base balance. Although the osteocyte-bone lining cells system demonstrated the regulatory role of the microenvironment homeostasis in these processes, the exact molecular mechanisms behind these processes remain unclear. CFTR is key to fluid homeostasis in epithelial cells/tissues. Mutations of CFTR results in bone problems both in humans and mice, although the exact role of CFTR in bone physiology remains unclear. Therefore, we

hypothesized that CFTR, through its channel function in conducting $\text{Cl}^-/\text{HCO}_3^-$ in bone cells, might play an important role in regulating the homeostasis of bone cell microenvironment.

Chapter 2. Methodology

2.1 Cell culture

MLO-Y4 (Karafast, EKC002) cells with passage number between 10-20 were cultured in alpha-Minimum Essential Media (Gibco, 11900024) and supplemented with 5% Fetal Bovine Serum, 1% penicillin and streptomycin (Gibco, 15140122) in the incubator with 37°C and humidified atmosphere of 95% air and 5% CO₂. Cells were maintained within 70% confluence and cultured on 0.15 mg/ml rat tail type 1 collagen (ThermoFisher, Cat. A1048301) coated dishes or flasks.

MC3T3 (ATCC, CRL-2593) cells with passage number between 10-20 were cultured in alpha-Minimum Essential Media (Gibco, 11900024) and supplemented with 10% Fetal Bovine Serum, 1% penicillin and streptomycin in the incubator with 37°C and humidified atmosphere of 95% air and 5% CO₂.

2.2 CFTR knockdown

CFTR knockdown was realized by using Small interfering RNA (siRNA). Before the transfection, MLO-Y4 cells were seeded at density of 2×10^4 cells/cm² on 35mm culture dishes with 25mm coverslips (Thermo Scientific, 11956528). After 24h, cells were transfected with 100nM Stealth™ RNAi duplexes targeting mouse CFTR (Thermo Scientific™, 1320001: MSS202938, 5'-GAG AUU GAU GGU GUC UCA UGG AAU U-3', siRNACFTR) or Low GC Stealth™ RNAi negative control duplexes (Thermo Scientific™, 12935200, siRNANC) as control with Lipofectamine™ 2000 (Invitrogen™, 11668027) in OptiMEM medium (Gibco, 31985088) according to the manufacturer's instructions. After 8-12 hr, transfected medium was replaced by regular culture medium. Experiment was conducted after additional 24 hr.

2.3 CFTR knockout by CRISPR-Cas9

MLO-Y4 cells with CFTR knockout were designed and completed by Peijie Hu from Dr Yechun Ruan's research group. The CFTR knockout was realized by CRISPR-Cas9 system. Guiding sgRNA was designed to target exon4, exon6 and exon8 of mouse CFTR sequence. All sgRNA was designed by using online tools (<https://portals.broadinstitute.org/>) and synthesized by Thermo Scientific™ (Table 2). sgRNA oligos were annealed and inserted into the plasmid MLM3636 (addgene, 43860). To verify the design, the recombinant MLM3636-sgRNA targeting mouse CFTR (MLM-sgRNACFTR) were sent to BGI Group Corp., Ltd for sanger sequencing. Before the transfection, MLO-Y4 cells were seeded at density of 1.0×10^4 cells/cm² for 24h. 0.5 µg recombinant MLM-sgRNACFTR 1 µg pSpCas9(BB)-2A-Puro (PX459) V2.0 (addgene, 62988) were transfected into cells with Lipofectamine™ 2000 (Invitrogen™, 11668027) in OptiMEM medium (Gibco, 31985088) according to the manufacturer's instructions. After observing 90% confluency of cell density, colony selection was achieved by adding 4µg/mL puromycin into the culture medium. After 72h, cells were seeded onto 96-well plate with density of 0.5 cells/well for single colony expansion. After 7 days, selected cells from one 96-well plate were seeded into 6-well plate for genomic DNA extraction by using GeneJET Genomic DNA Purification Kit (Thermo Scientific™, K0721).

Table 2. sgRNA targeting mouse CFTR

sgRN	Target	Forward (5'-3')*	Reverse (5'-3')*
A	ed exons		
1	4	ACACCGATTTTTGGCCTTCATCG CATG	AAAACATGCGATGAAGGCCAAA AATCG
2	6	ACACCGCCTTGGTTTACTGATA ATCCG	AAAACGGATTATCAGTAAACCA AGGCG
3	8	ACACCGTACCATATCTGTACGG CAGTG	AAAACACTGCCGTACAGATATGG TACG

2.4 RNA extraction and quantitative PCR

To extract the RNA from cells for the gene expression, culture medium was removed first. 500 μ L TRIzol (Invitrogen, 15596018) was added to each culture ware with repeated pipette up and down and samples were collected into RNase-free microtubes (Axygen, MCT-175-C). Follow the instruction of manufacturer, RNAs were extracted and assessed by Nanodrop spectrophotometer (Thermo, ND-ONE-W) to determine the purity and quantity. By using High-Capacity cDNA Reverse Transcription Kit (Thermo, 4368814), 1000ng RNA was reverse-transcribed to obtain corresponding cDNA. To conduct the quantitative PCR analysis, 1 μ l cDNA of each sample was added in the 10- μ l reaction system mixed with the SYBR Green Premix Ex Taq™ Mix (Takara, RR420A) and primers using the Bio-Rad real-time PCR system (Bio-Rad, CFX96). The results of the relative gene expression were normalized to *GUSB* and calculated by the $2^{-\Delta\Delta C_q}$ formula.

List of primers for qPCR

Gene Name	Forward (5' - 3')	Reverse (5' - 3')
Cftr	GCTGACACTTTGCTTGCCCTGAG	GCTTGCTGATGGTCGACATAGGG
Ptgs2	GGCGCAGTTTATGTTGTCTG	CAGCACTTCACCCATCAGTT
Tnfrsf11b	GAGACCAGGAAATGGTGAAG	CTCTCCATCAAGGCAAGAAG
Tnfsf11	CTGCAGGAGGATGAAACAA	CCATGAGCCTTCCATCATAG

2.5 RNA sequencing

To have a comprehensive gene profile of bone with CFTR deficiency, we conduct RNA sequencing for bone tissues from $\Delta F508$ - and wild-type mice. Conducted by Peijie Hu, RNA samples were extracted from the femora in 3-month-old $\Delta F508$ - and wild-type mice by RNeasy Mini Kit (Qiagen, 74104) following protocol illustrated by the manufacturer. RNA sequencing was completed by Novogene Co., Ltd with extracted RNA samples. There were 252,698,024 sequencing reads from three pair of wild-type and $\Delta F508$ - mice. Totally 88.79% of sequencing reads was mapped to the reference mouse genome using the STAR software. Considering sequencing depth and gene length of counted gene fragments, expression levels of targeted genes were represented by FPKM (fragments per kilobase of transcript sequence per millions base pairs sequenced)

Group	Wild-type			ΔF508		
Sample name	WT_1	WT_2	WT_3	ΔF_1	ΔF_2	ΔF_3
Total reads	43229852	40411338	43481810	39008326	38493644	43381666
Total mapped reads	26707478	38179896	41490300	34911826	36781208	41639862
Total mapping rate	61.78%*	94.47%	95.42%	89.5%	95.55%	95.99%

*Note: The sample from WT_1 was waived for analysis for the low mapping rate.

2.6 Patch-clamp recording

MLO-Y4 cells were cultured on 35mm culture dishes coated with rat tail type 1 collagen for 48 hours with the seeding density of 2,000/cm² before the patch-clamp recording. Borosilicate glass pipettes (Vitrex Micro-Haematocrit tubes, Modulohm A/S, DK-2730 Herlev, Denmark) were pulled and polished by Micropipette Pullers (P1000, Sutter Instrument Co., USA)

Glass pipette were filled with pipette solution to a resistance of 2-5M Ω after being immersed in bath solution. The ionic current was acquired by a Low-Noise Data Acquisition system (1550B, Axon™ Digidata®, Axon Instruments, USA) and amplified by the COMPUTER-CONTROLLED CURRENT and VOLTAGE CLAMP AMPLIFIER (700B, MultiClamp, Molecular Devices,

USA). Required voltage was commanded by pCLAMP 11 Software Suite. For the CFTR current measurement, cells were bathed in Margo ringers' solution (in mM): NaCl 130, KCl 5, MgCl₂ 1, CaCl₂ 2.5, Hepes 20 and glucose 5.8. (pH=7.4); pipette solution (CsCl 135, MgCl₂ 2, Mg-ATP 2, HEPES 10, EGTA 10, glucose 5.8). After the formation of Giga seal, the capacitance of cell was measured. Command voltage stepped from -80mV to +80mV (20mV increment) was applied to record the whole-cell current.

2.7 Membrane potential measurement

To measure the membrane potential (V_m), MLO-Y4 cells were cultured on 35mm culture dishes with 25mm coverslips (Thermo Scientific, 11956528). Before the measurement, cells were washed by Margo ringer's solution (in mM): NaCl 130, KCl 5, MgCl₂ 1, CaCl₂ 2.5, Hepes 20 and glucose 5.8. (pH=7.4). Next, cells on the coverslips were transformed and mounted on a mini chamber supplemented with 1ml bath solution with 2.5 μ M voltage-sensitive dye DiBAC4(3). Then, with a fluorescence microscope (Eclipse Ti, Nikon, Tokyo, Japan) the fluorescence (495/520 nm excitation/emission) was applied to the mini chamber at room temperature. The increased fluorescence intensity means depolarization of membrane potential, while decreased fluorescence intensity means hyperpolarization. To calibrate the change of fluorescence intensity into membrane potential (mV), incremental concentrations of potassium gluconate (5, 10, 20, 40 and 60 mM) was used to induce corresponded depolarization supplemented with valinomycin (2 μ M). The expected membrane potential changed by increased extracellular potassium was calculated by Nernst equation with the assumption of intracellular potassium concentration of 120 mM. The calibration curve was converted by fitting the fluorescence intensity change (% basal level).

2.8 Intracellular calcium measurement

To measure the intracellular calcium, MLO-Y4 cells were cultured on 35mm culture dishes with 25mm coverslips. Before the measurement, cells were washed by Margo ringer's solution (in mM): NaCl 130, KCl 5, MgCl₂ 1, CaCl₂ 2.5, Hepes 20 and glucose 5.8. (pH=7.4). Then, cells were incubated by Fura-2-AM (2.5μM) in the bath solution in 37° C for 30 mins. Next, cells washed by bath solution on the coverslips and transformed to a mini chamber supplemented with 1ml bath solution. After 15-minute stabilization, the mini chamber was mounted on a fluorescence microscope (Eclipse Ti, Nikon, Tokyo, Japan). Fluorescence was alternatively excited by dual wavelength at 340 and 380 nm, and emission signals were recorded at 510 nm. Intracellular calcium level was reflected by fluorescence intensity ratio of 340/380 nm.

2.9 Intracellular chloride measurement

To measure the intracellular chloride, MLO-Y4 cells were cultured on 35mm culture dishes with 25mm coverslips. Before the measurement, cells were washed by Margo ringer's solution (in mM): NaCl 130, KCl 5, MgCl₂ 1, CaCl₂ 2.5, Hepes 20 and glucose 5.8. (pH=7.4). Then, cells were incubated by halide-sensitive fluorescent dye N-(ethoxycarbonylmethyl)-6-methoxyquinolinium bromide (MQAE, 10mM) in the bath solution in 37° C for 30 mins. Next, cells washed by bath solution on the coverslips and transformed to a mini chamber supplemented with 1ml bath solution. After 15-minute stabilization, the mini chamber was mounted on a fluorescence microscope (Eclipse Ti, Nikon, Tokyo, Japan). Fluorescence was excited by 340 nm, and emission signals were recorded at 460. The MQAE was a quenching dye, with increased MQAE fluorescence intensity means decreased intracellular chloride, whereas decreased MQAE fluorescence intensity means increased intracellular chloride.

2.10 Ultrasound stimulation for gene expression analysis

MLO-Y4 cells were cultured on 6-well culture plates with the density of 1×10^4 cells/cm² for 24hrs before the treatment with Low intensity pulsed ultrasound (LIPUS), 1.5 MHz, 200ms pulsed-wave mode intensity of 30 mW/cm² (EXOGEN, USA). Before the treatment, the culture plate was smeared with a layer of ultrasound gel (Aquasonic Clear Ultrasound Transmission Gel). During the stimulus of LIPUS (20min, 1hr and 3hrs), cells were maintained at the incubator with 37°C and humidified atmosphere of 95% air and 5% CO₂. Samples were collected after the treatment of LIPUS.

2.11 Ultrasound stimulation for intracellular ions measurement

The ultrasound stimulation system borrowed from Prof. Sun Lei's group consisted of a commercial transducer (I7-0012-P-SU, Olympus), two function generators, and a power amplifier (Electronics and Innovation, A075). This device generates 200 tone burst pulses with frequency of 0.5MHz and a duty cycle of 40%. The output intensity was limited to 0.1 - 0.5 MPa. The transducer was immersed in the bath solution vertically during the measurement of calcium imaging.

2.12 Statistics

Data are represented as mean \pm s.e.m. Two-tail unpaired Student's t-tests were used for comparison between two groups. A probability of $P < 0.05$ was considered to be statistically significant.

Chapter 3. Results

3.1 CFTR mediates Cl⁻ efflux in MLO-Y4 cells.

3.1.1 Channel function of CFTR conducting Cl⁻

To identify the CFTR function as the Cl⁻ channel in osteocytes, we first monitored the whole-cell currents in an osteocyte-like cell line, MLO-Y4 cells, by applying the patch-clamp technique. Before the whole-cell currents measurement, the pulled borosilicate glass pipette was filled with prepared pipette solution (Detailed components were described in method 2.6). After fixing it in the pressure regulator associated with a motorized manipulator, small positive pressure was applied to the pipette by a connected syringe. Controlled by the motorized manipulator, the glass pipette slowly moved down until the tip of it was immersed in the bath solution. After manipulating the glass pipette to approach the targeted cell, a bright pit on the cellular membrane can be observed. By releasing the positive pressure in the syringe, a seal with high resistance (Giga Ohm) would form between the cell membrane and the patching tip of the glass pipette. A negative pressure was subsequently applied to break the patched membrane and make the intracellular fluid mixed with the pipette solution. We latterly detected a inward current in the MLO-Y4 cells (Holding voltage:-60mV) after 7-10 minutes of the treatment of adenylyl cyclase activator, forskolin (10 μM), which could be inhibited by the CFTR inhibitor, CFTR_{inh}-172 (10 μM) (Fig. 3.1.1 A). After observing the stable inward current, command voltage (Sustaining for 700ms) stepped from -80mV to +80mV (20mV increment) was applied to patched cells. Under 1-sec stimuli of stepped voltages, voltage- and time- independent currents were observed (Fig. 3.1.1 B). By plotting the results from stepped-voltage-induced currents into I-V curve (Fig. 3.1.1 C), a linear characteristic curve suggested that the observed inward current was mediated by an ion channel. Besides, the reversal

potential measured in the I-V curve was close to Cl^- determined one, which calculated by the Nernst potential. It suggested that the ion channel was a Cl^- ion channel sensitive to both forskolin and $\text{CFTR}_{\text{inh-172}}$. Collectively, these observations suggested that the forskolin-activated currents were mediated by CFTR.

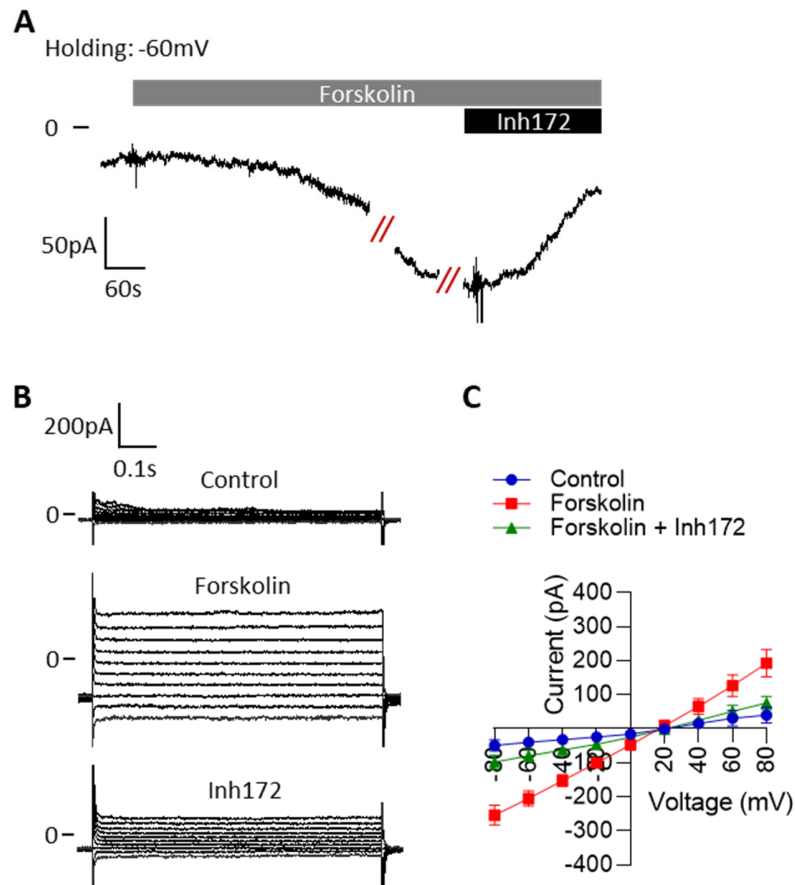


Figure 3.1.1. Channel function of CFTR in MLO-Y4 cells. (A) With holding voltage at -60mV, Forskolin (10 μM) induced inward currents were blocked by $\text{CFTR}_{\text{inh-172}}$ (10 μM) in osteocyte-like cell line, MLO-Y4 cells (B) Currents measured under commanding voltage stepped from -80mV to +80mV with 20mV increment and lasting for 700ms. (C) I-V curve of currents activated by commanding voltage steps. (n=3)

3.1.2 Effect of the CFTR inhibitor on intracellular Cl⁻ concentration and membrane potential

Although we successfully recorded CFTR currents in MLO-Y4 cells, the direction of the Cl⁻ flux was unclear. To investigate it, we next examined the involvement of CFTR in regulating intracellular chloride by a fluorometric method in MLO-Y4 cells. After supplementing MLO-Y4 cells with CFTR inhibitor, CFTR_{inh}-172 (10 μM), the fluorescence intensity of MQAE, a fluorescent quenching indicator for intracellular chloride, was significantly decreased (Fig. 3.1.2 A). To monitor the variation of the intracellular chloride in MLO-Y4 cells, we converted the change of MQAE fluorescence intensity (%basal) into change of intracellular chloride ($\Delta[\text{Cl}^-]_i$ mM) by the calibration curve (Fig. 3.1.2 B). Both two different CFTR inhibitors, GlyH-101 (1, 10 μM) and CFTR_{inh}-172 (1, 10 μM) significantly increased the intracellular chloride in MLO-Y4 cells in a dosage-dependent manner (Fig. 3.1.2 B). It indicated that the $[\text{Cl}^-]_i$ in MLO-Y4 cells could be increased by CFTR-inhibitor-induced net Cl⁻ influx, which suggested that CFTR contributed to the Cl⁻ efflux in MLO-Y4 cells under regular conditions.

As CFTR was reported to be involved in the membrane potential maintenance (Guo et al., 2014), we further asked whether the CFTR-mediated Cl⁻ efflux was associated with the membrane potential variation in MLO-Y4 cells. Using the voltage-sensitive dye DiBAC₄(3) (Bis-(1,3-Dibutylbarbituric Acid) Trimethine Oxonol), we observed decreased fluorescence intensity of DiBAC₄(3) in MLO-Y4 cells after the treatments of CFTR inhibitors, CFTR_{inh}-172 (10 μM) (Fig. 3.1.2 C). To acquire the variation of the membrane potential in MLO-Y4 cells, we converted the change of DiBAC₄(3) fluorescence intensity (%basal) into change of membrane potential (V_m mV) by the calibration curve (Fig. 3.1.2 D). Both two different CFTR inhibitors, GlyH-101 (10 μM) and CFTR_{inh}-172 (10 μM) significantly hyperpolarized the intracellular chloride in MLO-Y4 cells (Fig. 3.1.2 D). The hyperpolarized membrane potential caused by the treatment of CFTR inhibitors

suggested that CFTR mediated the net Cl⁻ efflux across the cellular membrane in MLO-Y4 cells, which was consistent with results observed in CFTR inhibitors induced variation of MQAE fluorescence intensity.

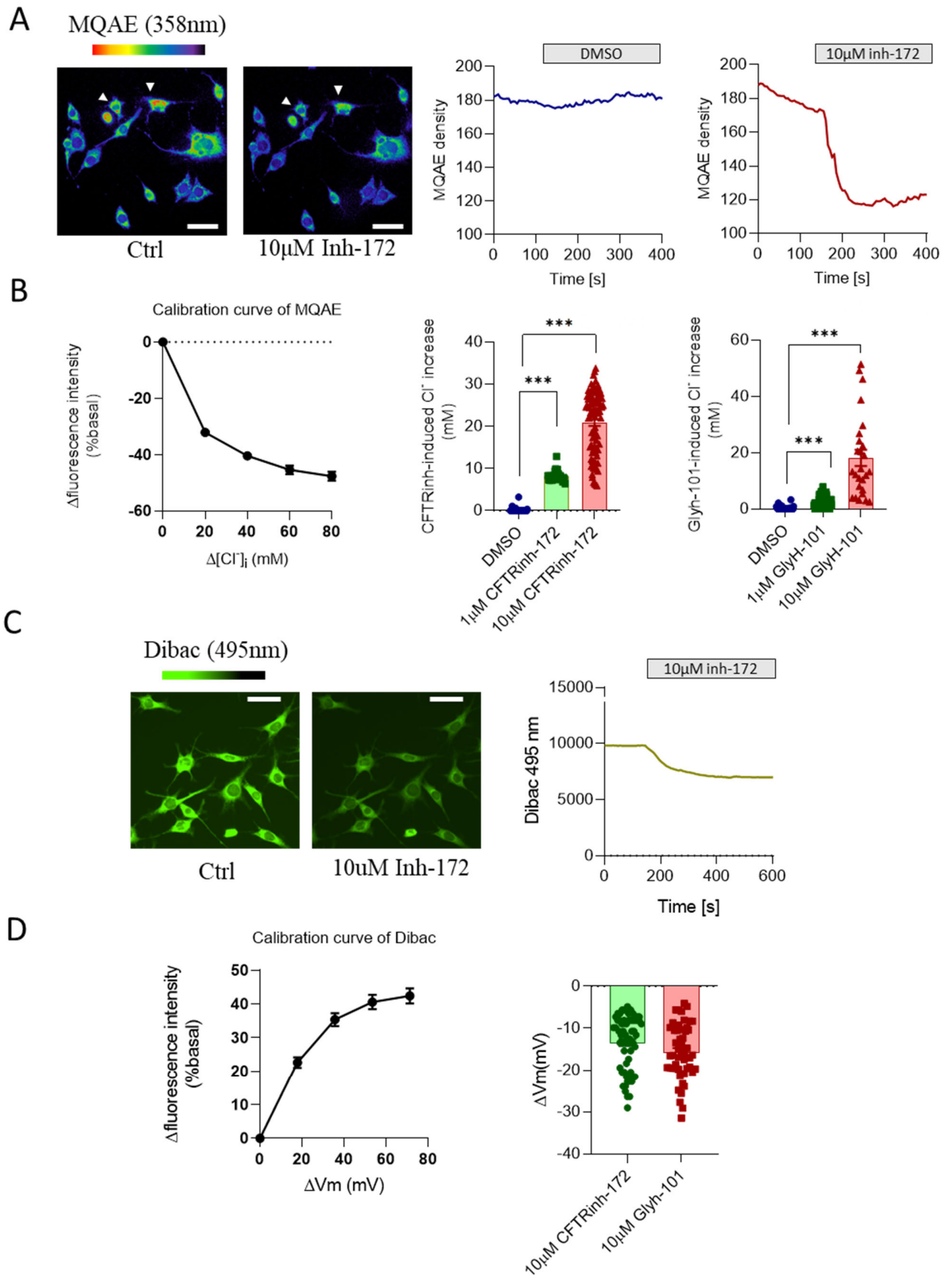


Figure 3.1.2. Effect of the CFTR inhibitor on $[Cl^-]_i$ and V_m . (A) Representative figures (left) and fluorometric curve (right) of intracellular Cl^- for MLO-Y4 cells. Controlled by DMSO, CFTR_{inh}-172 (10 μ M) decreased fluorescence intensity of Cl^- -sensitive dye MQAE. (B) Variation of fluorescence intensity (%) was converted to corresponding change of intracellular Cl^- concentration (mM) by the calibration curve of MQAE. CFTR inhibitors, CFTR_{inh}-172 (1, 10 μ M) and GlyH-101 (1, 10 μ M) significantly increased intracellular Cl^- concentration of MLO-Y4 cells in a dosage-dependent manner (right). Inhibitors were controlled by DMSO. Data are mean \pm s.e.m. *** $P < 0.001$ by t-test. Scale bars, 20 μ m. (C) Representative figures (left) and fluorometric curve (right) of membrane potential for MLO-Y4 cells. Controlled by DMSO, CFTR_{inh}-172 (10 μ M) decreased fluorescence intensity of membrane potential sensitive dye DiBAC₄(3). (D) Variation of fluorescence intensity (%) was converted to corresponding change of membrane potential (mV) by the calibration curve of DiBAC₄(3). CFTR inhibitors, CFTR_{inh}-172 (10 μ M) and GlyH-101 (10 μ M) significantly hyperpolarized the membrane potential of MLO-Y4 cells. Inhibitors were controlled by DMSO. Scale bars, 20 μ m.

3.1.3 Effect of CFTR knockout and knockdown on CFTR conducting Cl⁻

To verify the Cl⁻ efflux conducted by CFTR in MLO-Y4 cells, we first tried the CFTR-knockdown model in MLO-Y4 cells by small interfering RNA (siRNA). As CFTR_{inh}-172 could increase [Cl⁻]_i in MLO-Y4 cells by inhibiting the CFTR-mediated Cl⁻ efflux, we asked whether MLO-Y4 cells with CFTR knockdown could have less sensitivity to the treatment of CFTR_{inh}-172. Reflecting on the fluorometric measurement of intracellular Cl⁻ concentration, the change induced by CFTR_{inh}-172 of fluorescence intensity might be less in the group with CFTR knockdown compared to the small interfering negative control group. We monitored the change (%) of [Cl⁻]_i after the treatment of CFTR_{inh}-172 in MLO-Y4 cells with and without CFTR knockdown after 24 and 48 hours (Fig 3.1.3 A). Although there was no significant difference of the [Cl⁻]_i (MQAE fluorescence intensity) after the treatment of CFTR_{inh}-172 (10μM) between silencing negative control group and CFTR knockdown group after the 24-hours siRNA knockdown, the batch of cells after 48 hours show slightly decreased fluorescence intensity to the treatment of CFTR_{inh}-172 (10μM) in siRNA-treated group compared to control group. qPCR was later conducted to MLO-Y4 cells after 24-hour treatment of siRNA. Based on the mRNA expression level of CFTR in this model, no significant change between siRNA-treated group and control group was found even though some samples significantly lower than others (Fig 3.1.3 B). It indicated that our siRNA model might be not stable, which might explain the slight change of decreased MQAE intensity with statistical difference.

As an alternative strategy for verifying CFTR chloride ion channel function in osteocytes, we next applied CRISPR-Cas9 system for MLO-Y4 cells to establish a CFTR knockout model for osteocytes. To verify the Cl⁻ efflux conducted by CFTR in MLO-Y4 cells, we next repeated the whole-cell current recordings in MLO-Y4 cells with CFTR knockout. With the same pipette

solution and extracellular solution, no additional current was recorded in $Cftr^{-/-}$ MLO-Y4 cells (Fig 3.1.3 F,G, H n=3) while the forskolin-activated and CFTR_{inh}-172-blocked currents with similar characteristics as former records were observed in wild-type MLO-Y4 cells (Fig 3.1.3 C,D,E n=3). It indicated that it was CFTR responsible for mediating the forskolin- and CFTR inhibitor-sensitive current in MLO-Y4 cells.

To further verify the direction of the CFTR mediated Cl⁻-current flux, we next monitored the [Cl⁻]_i of MLO-Y4 cells with or without CFTR knockout by the same method described before. After the treatment of CFTR_{inh}-172 (10μM), we quantified and compared the inhibitor-induced [Cl⁻]_i change (mM) of [Cl⁻]_i in MLO-Y4 cells. We observed larger increase of [Cl⁻]_i in MLO-Y4 cells with CFTR knockout compared to the control group (Fig 3.1.3 I). This result suggested that CFTR mediated the Cl⁻ efflux in wild-type MLO-Y4 cells.

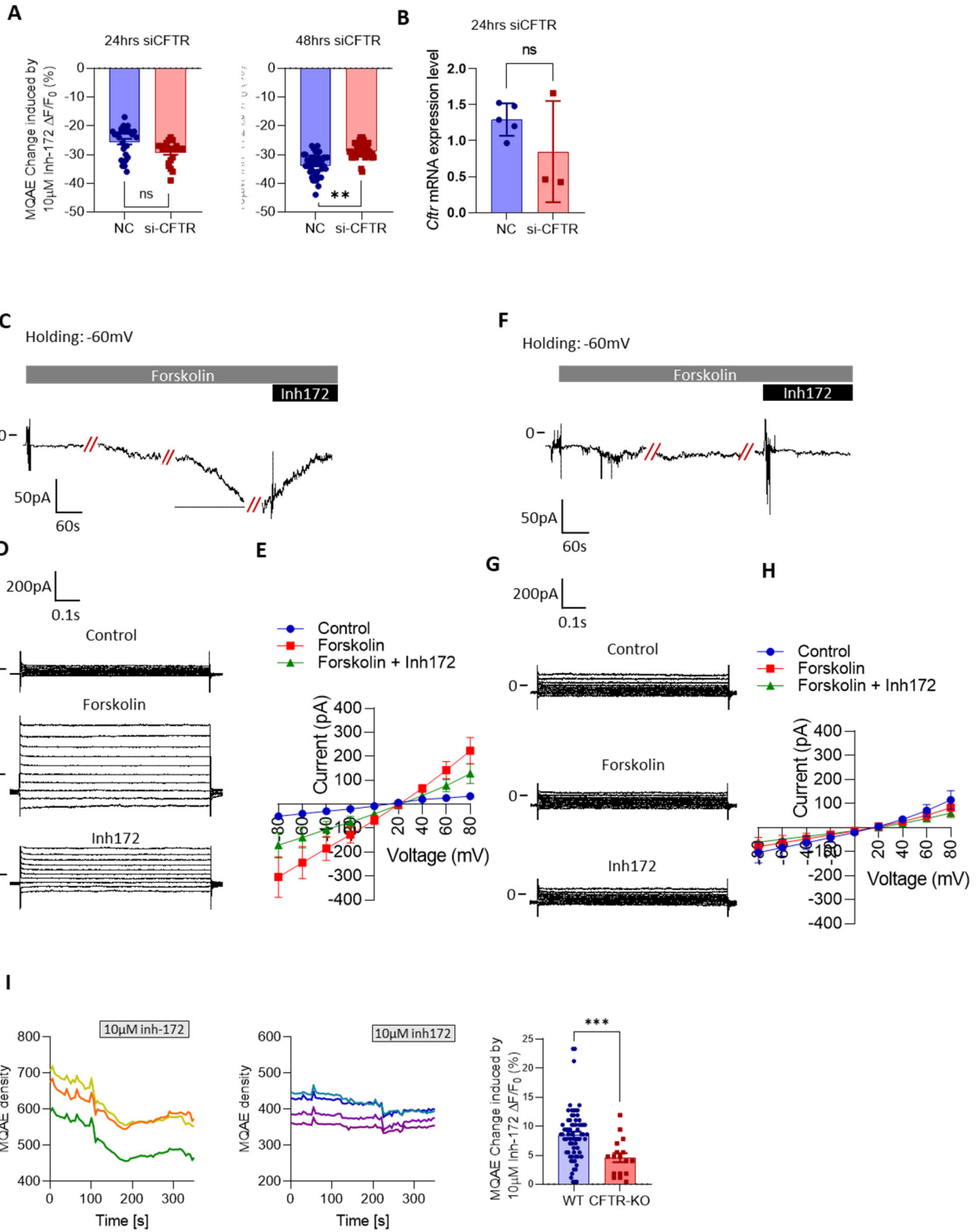


Figure 3.1.3. Effect of CFTR knockdown and knockout on CFTR channel function

(A) No significantly difference of CFTR_{inh-172} (10 μ M) induced variations of MQAE fluorescence intensity between CFTR-knockdown MLO-Y4 cells compared to control groups (24 and 48 hrs after the transfection). (B) qPCR analysis of CFTR expression in MLO-Y4 cells with (24 hrs after the transfection) or without si-CFTR transfection. (C) With holding voltage at -60mV, Forskolin (10 μ M) induced inward currents were blocked by CFTR_{inh-172} (10 μ M) in wild-type CFTR MLO-Y4 cells. (D) Currents measured under commanding voltage stepped from -80mV to +80mV with 20mV increment and lasting for 700ms. (E) I-V curve of currents activated by commanding voltage steps. (n=3) (F) With holding voltage at -60mV, no current was observed after the treatment of Forskolin (10 μ M) and CFTR_{inh-172} (10 μ M) in CFTR knockout MLO-Y4 cells (G) Recorded currents under commanding voltage stepped from -80mV to +80mV with 20mV increment and lasting for 700ms. (H) I-V curve of currents activated by commanding voltage steps (n=3). (I) Representative fluorometric curves of intracellular Cl⁻ for wildtype- and CFTR-knockout MLO-Y4 cells with treatment of CFTR_{inh-172} (10 μ M). CFTR_{inh-172} (10 μ M) induced significantly higher [Cl⁻]_i in wildtype MLO-Y4 cells compared to CFTR-knockout MLO-Y4 cells. Data are mean \pm s.e.m. ns $P > 0.05$, ** $P < 0.01$, *** $P < 0.001$ by t-test.

3.1.4 Summary

In the first session, we demonstrated the channel function of CFTR in MLO-Y4 cells mediating the Cl⁻ efflux. With the patch-clamp technique and fluorometric measurement, we found that 1) recorded whole-cell currents in MLO-Y4 cells were activated by forskolin and blocked by CFTR_{inh-172}. 2) CFTR_{inh-172} increased intracellular Cl⁻ concentration [Cl⁻]_i and depolarized membrane potential (V_m) in MLO-Y4 cells. 3) Change of intracellular Cl⁻ concentration [Cl⁻]_i

induced by CFTR_{inh}-172 (10μM) was significantly abolished in MLO-Y4 cells with CFTR knockout (Cfr^{-/-}). These consistent results indicated that CFTR plays the channel function by mediating the Cl⁻ efflux in MLO-Y4 cells.

3.2 CFTR contributes to pH regulation in osteocytes

3.2.1 Effect of the CFTR inhibitor on HCO₃⁻ secretion and pH maintenance in MLO-Y4 cells.

As an anion channel, CFTR was reported to demonstrate the permeability of HCO₃⁻ and contributed to pH regulation in other tissues (Park et al., 2010). To have a comprehensive understanding of CFTR channel function in osteocytes, we assessed the capability of CFTR conducting HCO₃⁻ in MLO-Y4 cells. By using pH-sensitive fluorometric dye BCECF [2',7'-bis-(2-carboxyethyl)-5-(and-6)-carboxyfluorescein], the HCO₃⁻ flux in MLO-Y4 cells was indirectly measured by the pH recovery rate after intracellular alkalization induced by removing saturated HCO₃⁻/CO₂ from the bath solution of MLO-Y4 cells. MLO-Y4 cells incubated with BCECF (2.5 μM) were initially perfused by HEPES (4-(2-hydroxyethyl)-1-piperazineethanesulfonic acid)-buffer solution, which maintained the physiological pH of MLO-Y4 cells around 7.4 under the ambient atmosphere. After substituting the HEPES-buffer solution with saturated HCO₃⁻/CO₂ solution, intracellular pH (Ratio of BCECF 495nm/436nm) of MLO-Y4 cells acutely dropped down (Fig 3.2.1 B. a') due to the increased [H⁺]_i produced by intracellular carbonic acid. Subsequently, saturated HCO₃⁻/CO₂ solution was replaced back to HEPES-buffer solution and induced the dramatical increment of intracellular pH in MLO-Y4 cells (Fig 3.2.1 B. b'). Following the intracellular alkalization, intracellular pH was slowly decreased in MLO-Y4 cells (Fig 3.2.1 B. c'). Within the process of MLO-Y4 cells pH self-recovery from the alkalization, interference of Cl⁻/HCO₃⁻ exchanger for HCO₃⁻ secretion Cl⁻ was removed by substituting Cl⁻ to gluconate ion in all bath solution for MLO-Y4 cells. Supplemented with CFTR inhibitor, CFTR_{inh}-172 (10 μM), we observed significantly attenuated pH recovery rate after the intracellular alkalization represented by the slope of the pH curve (Fig 3.2.1 B). This slower slop indicated a CFTR inhibitor caused decrement of HCO₃⁻ secretion, which suggested that CFTR contributed to HCO₃⁻ secretion

in MLO-Y4 cells. This observation supported the permeability of CFTR for HCO_3^- and enhanced our understanding of the CFTR channel function in MLO-Y4 cells.

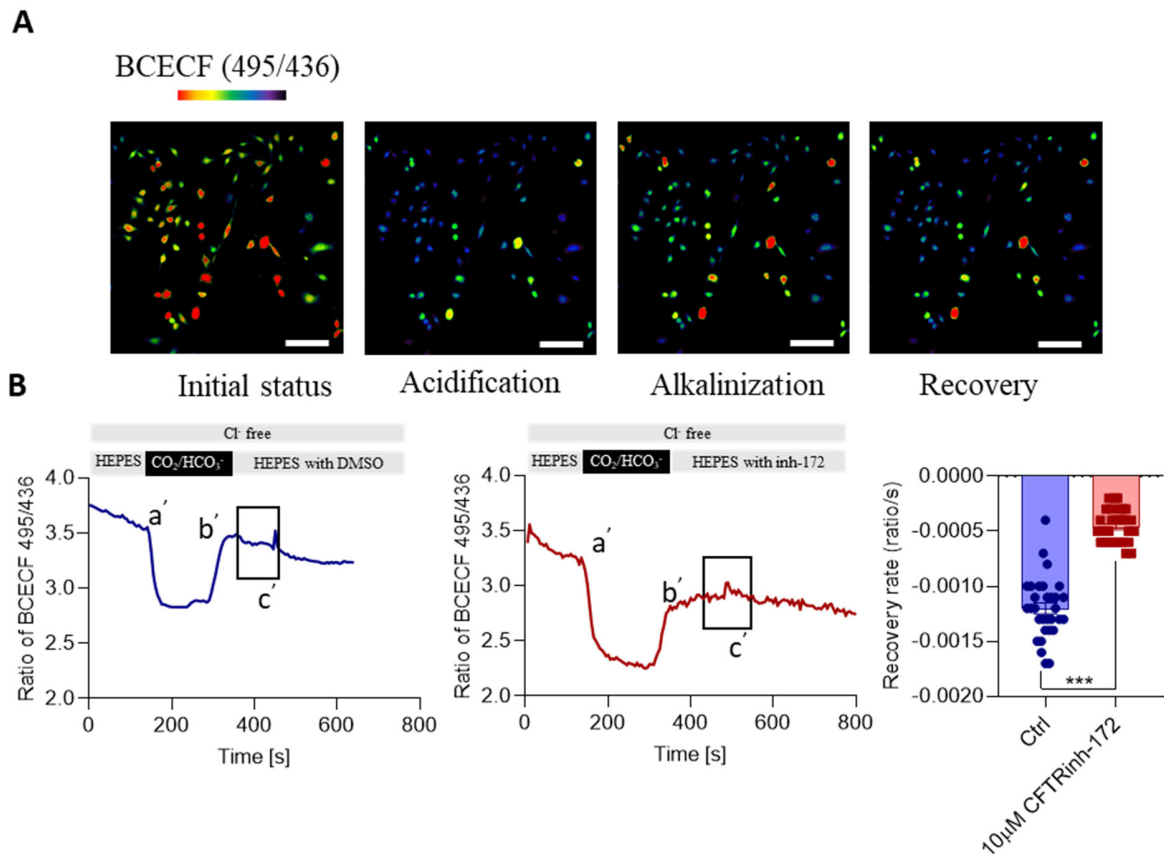


Figure 3.2.1. Effect of the CFTR_{inh}-172 on HCO_3^- secretion and pH maintenance in MLO-Y4 cells (A) Representative figures and fluorometric curves (B) of intracellular pH (Ratio of BCECF, 495nm/436nm) for MLO-Y4 cells. After replacing the bath solution with HEPES buffer by solution perfused with saturated CO_2 gas, ratio of BCECF (495nm/436nm) was decreased (acidification). After changing the bath solution back to HEPES buffered solution, ratio of BCECF (495nm/436nm) increased (alkalinization) and slowly decreased (pH recovery) to a stable value. (B) HCO_3^- secretion was indirectly measured by the pH recovery rate. Within the black rectangle area, recovery rate was calculated by the ratio/s. Controlled by DMSO, CFTR_{inh}-172 (10µM)

significantly decreased the recovery rate in MLO-Y4 cells. Data are mean \pm s.e.m. *** $P < 0.001$ by t-test. Scale bars, 100 μ m.

3.2.2 Effect of CFTR knockout on HCO₃⁻ secretion and pH maintenance in MLO-Y4 cells.

To verify the reduced HCO₃⁻ secretion caused by CFTR_{inh-172} in MLO-Y4 cells, we measured and compared the slope of pH recovery rate after the intracellular alkalization in MLO-Y4 cells with and without CFTR knockout. With the same condition, we monitored the change of intracellular pH in MLO-Y4 cells by pH-sensitive fluorometric dye BCECF (2.5 μ M). After replacing the HCO₃⁻/CO₂ pulsion with HEPES-buffer solution, the slope of the pH-recovery curve changing from the intracellular alkalization was significantly smoother in MLO-Y4 cells with CFTR knockout compared to wild-type MLO-Y4 cells (Fig 3.2.2 A b'). It confirmed the functional role of CFTR in secreting HCO₃⁻ in MLO-Y4 cells.

Besides, we also observed a significant difference of the slope of pH curve recovering from intracellular acidification between wild-type and CFTR-knockout MLO-Y4 cells (Fig 3.2.2 A a'). It suggested that the wild-type MLO-Y4 cells tended to recover their intracellular pH from the acidification while the CFTR-knockout MLO-Y4 cells seemed to maintain a stable acidified pH value when perfused in saturated CO₂ atmosphere. This result pointed out that wild-type MLO-Y4 cells might adapt themselves by secreting the retained intracellular protons while CFTR-knockout MLO-Y4 cells showed less ability to mobilize the accumulated protons.

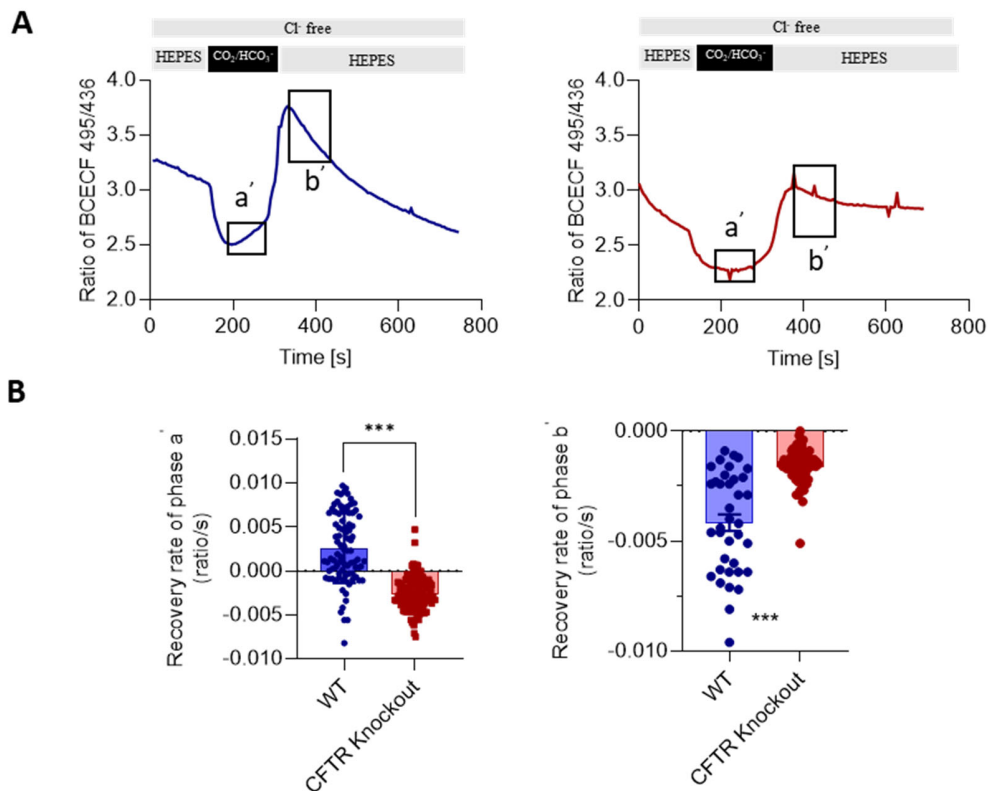


Figure 3.2.2. Effect of CFTR knockout on HCO₃⁻ secretion and pH maintenance in MLO-Y4 cells (A) Representative curves of intracellular pH (Ratio of BCECF, 495nm/436nm) for wild-type and CFTR-knockout MLO-Y4 cells. After replacing the bath solution with HEPES buffer by solution perfused with saturated CO₂ gas, ratio of BCECF (495nm/436nm) was decreased (acidification). After changing the bath solution back to HEPES buffered solution, ratio of BCECF (495nm/436nm) increased (alkalization) and slowly decreased (pH recovery) to a stable value. (B) H⁺ and HCO₃⁻ secretion was indirectly measured by the pH recovery rate within the black rectangle area (a' and b'). Data are mean ± s.e.m. ****P*<0.001 by t-test.

3.2.3 Involvement of CFTR in pH recovery from intracellular acidification in osteocytes

To explain the weakened ability to mobilize the accumulated protons in CFTR-knockout MLO-Y4 cells (Fig 3.2.2 A a'), we hypothesized that CFTR was correlated to proton pumps (vacuolar-ATPase) regulating intracellular protons, which were responsible for the mobilization of intracellular protons in MLO-Y4 cells. To verify this hypothesis, we next conducted an RNA-seq analysis of all subunits of vacuolar-ATPase in bone tissues derived from DF508 and wild-type mice to explore the potential interaction between CFTR and vacuolar-ATPase. Among these subunits, the expression level of *Atp6v1d*, *Atp6v1g2*, and *Atp6v0d2* were significantly downregulated, while other subunits were slightly downregulated without significant value (Fig. 3.2.3 A).

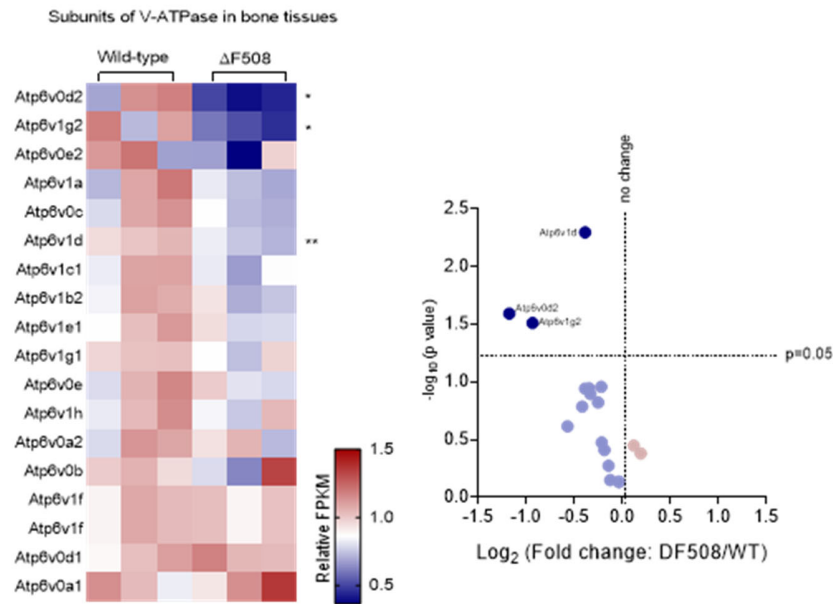
A

Figure 3.2.3. RNA-seq analysis of bone tissues in DF508 and wild-type mice (a) RNA-seq analysis of heatmap (left) and Volcano plot (right) with the \log_2 fold changes in gene expression of all subunits of V-ATPase in bone tissues showed that some genes of subunits were significantly downregulated in $\Delta F508$ mice compared to wild-type mice. Data are mean \pm s.e.m. * $P < 0.05$, ** $P < 0.01$ by t-test.

3.2.3 Summary

In this session, we demonstrated the channel function of CFTR in MLO-Y4 cells mediating HCO_3^- secretion and possible correlation to proton pumps for pH regulation. With the fluorometric measurement and RNA-Seq technique, we found that 1) CFTR_{inh}-172 impeded the pH recovery rate of MLO-Y4 cells from intracellular alkalization by inhibiting the HCO_3^- exclusion of CFTR. 2) Genes encoding subunits of Vacuolar-type ATPase (V-ATPase) were significantly upregulated

in bones from mice with CFTR deficiency compared to wild-type mice. These results collectively suggested that CFTR involves in pH regulation in the microenvironment for osteocytes.

3.3 Involvement of CFTR in mechanotransduction in MLO-Y4 cells

3.3.1 CFTR involved in ultrasound-induced gene expressions in MLO-Y4 cells

To investigate the mechanosensitivity of CFTR in MLO-Y4 cells, we first analyzed the correlation between *Cftr* and key genes relative to osteocytes mechanotransduction by qPCR in MLO-Y4 cells after the treatment of LIPUS. Three time periods (20 minutes, 1 and 3 hours) of LIPUS were selected as the test dosage of ultrasound to obtain a comprehensive profile of genes expression in MLO-Y4 cells. Based on our results, we found that *Cftr* was only upregulated by 20-min treatment of LIPUS while *COX-2* and ratio of *OPG/RANKL* were upregulated after 3-hour treatment (Fig. 3.3.1 A). It indicated that *Cftr* was upregulated prior to *COX-2* of MLO-Y4 cells at mRNA level and might be required for LIPUS-induced mechanotransduction.

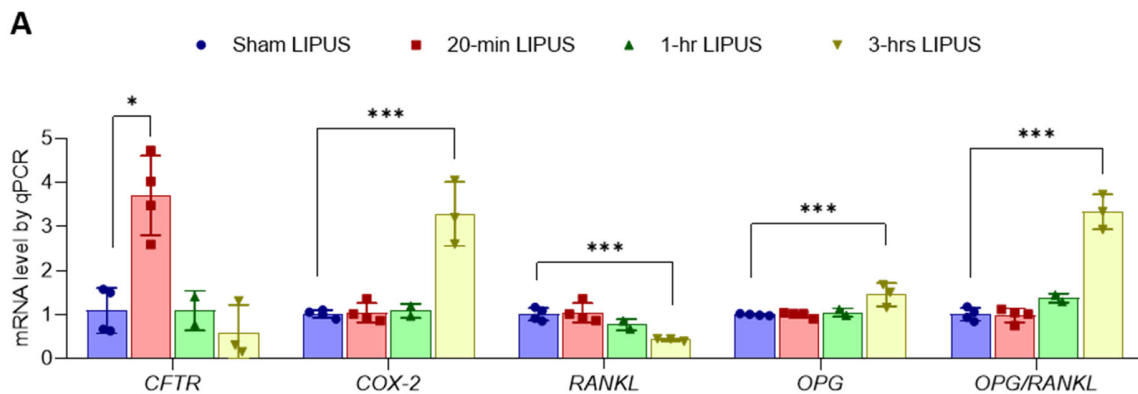


Figure 3.3.1 qPCR analysis of MLO-Y4 cells after the ultrasound stimulation.

(A) qPCR results for CFTR, key genes for mechanotransduction (COX-2) and key genes for regulating bone turnover (OPG and RANKL) after the treatment of LIPUS for 20 minutes, 1 hour and 3 hours. Data are mean \pm s.e.m. * P <0.05, *** P <0.001 by t-test.

3.3.2 Effects of the CFTR inhibitor on ultrasound-induced change of intracellular Ca^{2+} and Cl^- concentrations in MLO-Y4 cells.

As the central regulator of bone mechanotransduction, osteocytes were also involved in a mechano-induced endocrine pathway. Among several molecules, PGE_2 catalysed by COX-2 was the essential component for osteocyte mechanotransduction, and its synthesis was promoted by Ca^{2+} influx through the voltage-sensitive complex activated by mechanical stimulus or membrane depolarization (Yavropoulou, Yovos, & interactions, 2016). That means, $[\text{Ca}^{2+}]_i$ was critical for the osteocytes mechanotransduction.

To further investigate whether CFTR was involved in the mechanotransduction of osteocytes, we analysed effects of $\text{CFTR}_{\text{inh-172}}$ on the $[\text{Ca}^{2+}]_i$ by calcium-sensitive fluorescent dye Fura-2-AM (2.5 μM) in MLO-Y4 cells under ultrasound stimulus (Detailed specifications of the ultrasound were described in method). As shown in Fig. 3.3.2 A and B, MLO-Y4 cells demonstrated timely increment of $[\text{Ca}^{2+}]_i$ to ultrasound stimulus in a dosage-dependent manner (0.1 - 0.5 MPa). However, MLO-Y4 cells supplemented with $\text{CFTR}_{\text{inh-172}}$ (10 μM) showed inhibited calcium response (Fig. 3.3.2 B). Including calcium response, we next monitored the $[\text{Cl}^-]_i$ in MLO-Y4 cells under the ultrasonic stimulation to explore the involvement of mechano-sensitivity of CFTR in the mechanotransduction. Similar as the calcium response, $[\text{Cl}^-]_i$ varied timely upon the ultrasonic stimulation in a dosage-dependent manner (0.1-0.5 MPa) and the ultrasound-induced change of $[\text{Cl}^-]_i$ can be blocked by $\text{CFTR}_{\text{inh-172}}$ (10 μM) (Fig. 3.3.2 C and D).

It suggested that increased $[Cl^-]_i$ by CFTR_{inh}-172 could not be further affected by the stimulation of the ultrasound.

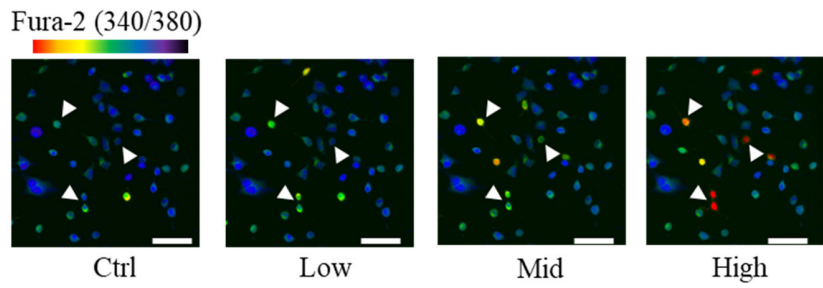
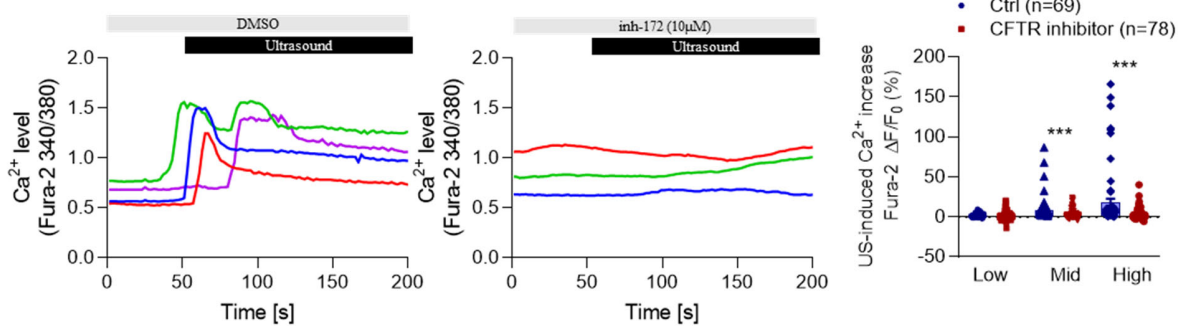
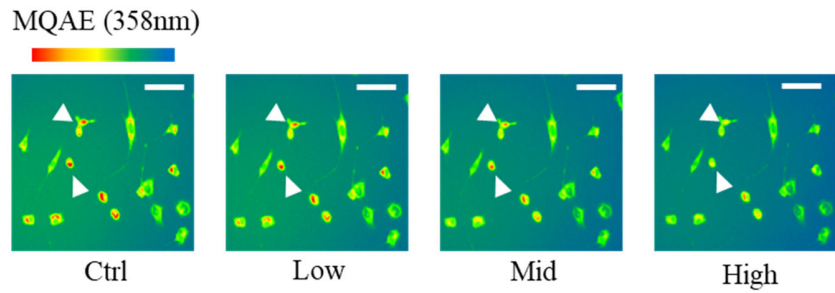
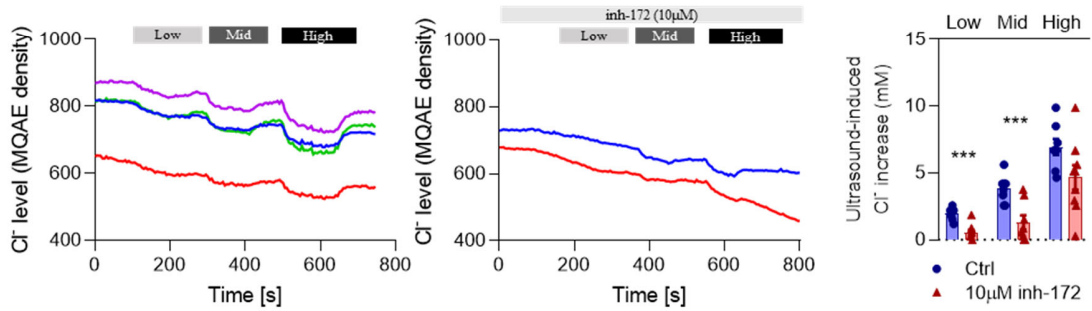
A**B****C****D**

Figure 3.3.2 Effects of the CFTR inhibitor on ultrasound-induced change of $[Ca^{2+}]_i$ and $[Cl^-]_i$ in MLO-Y4 cells. (A) Representative figures and (B) curves of calcium imaging of Fura-2-AM-loaded MLO-Y4 cells. MLO-Y4 cells were sensitive to ultrasound stimulus in a dosage-dependent manner and increments of $[Ca^{2+}]_i$ could be inhibited by CFTR_{inh}-172 (10 μ M). Data are mean \pm s.e.m. *** $P < 0.001$ by t-test. Scale bars, 100 μ m (C) Representative figures and (D) curves of calcium imaging of MQAE-loaded MLO-Y4 cells. MLO-Y4 cells were sensitive to ultrasound stimulus in a dosage-dependent manner and increments of $[Cl^-]_i$ could be inhibited by CFTR_{inh}-172 (10 μ M). Data are mean \pm s.e.m. *** $P < 0.001$ by t-test. Scale bars, 100 μ m

3.3.3 Effects of CFTR inhibitors on stretch-induced gene expressions in MLO-Y4 cells

Osteocytes in lacuna-canalicular systems suffered from various mechanical stimuli, including flowing shear stress and deformation-caused strain (Chen, Liu, You, & Simmons, 2010). We applied stretching force as additional mechanical stimulus to MLO-Y4 cells exploring the mechanosensitive involvement of CFTR in mechanotransduction of osteocytes. Demonstrated by the qPCR analysis, although the stretching-induced upregulation of COX-2 could be blocked by both CFTR_{inh}-172 (10 μ M) and GlyH-101 (10 μ M), the expression of CFTR seemed independent on the stretching force (Fig 3.3.3 A). Different from what we observed in qPCR results of ultrasound-induced gene expression, RANKL was significantly upregulated through the stimulation of stretch and downregulated by CFTR inhibitors while no significant change was observed for OPG (Fig 3.3.3 B).

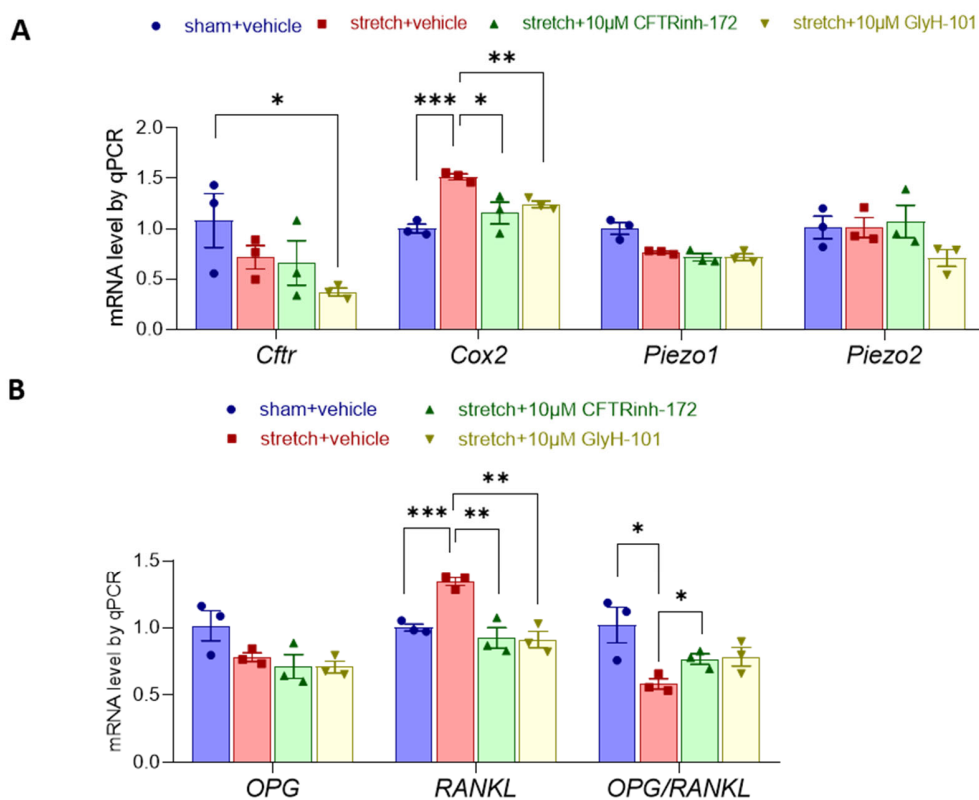


Figure 3.3.3 Effects of CFTR inhibitors on stretch-induced gene expressions in MLO-Y4

cells (A) qPCR results for CFTR, mechanosensitive channels (Piezo 1 and 2), key gene for mechanotransduction (COX-2) and Data are mean \pm s.e.m. * P <0.05, ** P <0.01, *** P <0.001 by t-test. (B) key genes for regulating bone turnover (OPG and RANKL) after the treatment of cyclic stretch (60 cycles/hour) with/without CFTR inhibitors (CFTR_{inh}-172, GlyH-101, 10 μ M) for 1 hour. Data are mean \pm s.e.m. * P <0.05, ** P <0.01, *** P <0.001 by t-test.

3.3.4 Summary

In this session we investigated the mechano-sensitivity of CFTR in the mechanotransduction of MLO-Y4 cells. With the ultrasound stimuli, we found that 1) CFTR mRNA level was upregulated in advance to COX-2 in MLO-Y4 cells. 2) Ultrasound-induced Ca²⁺ and Cl⁻ response could be blocked by CFTR_{inh}-172 (10 μ M) 3) CFTR_{inh}-172 (10 μ M) and GlyH-101 (10 μ M) blocked stretch-induced upregulation of COX-2 at mRNA level. These results suggested that CFTR might involve in the mechanotransduction of MLO-Y4 cells via its mechano-sensitive property.

3.4 Comparison of CFTR channel functions between MLO-Y4 cells and MC3T3 cells.

3.4.1 Effect of the CFTR inhibitor on intracellular Cl⁻ concentration and membrane potential in MLO-Y4 cells and MC3T3 cells.

Based on the results derived from patch-clamp and fluorometric techniques, CFTR demonstrated channel functions in the osteocyte-like cell line MLO-Y4 cells by mediating Cl⁻ efflux and HCO₃⁻ secretion. As the cellular basis compartmentalizing the BECF and ECF, bone lining cells are essential for the homeostasis of BECF. To have a comprehensive understanding of the involvement of CFTR in the regulation of BECF homeostasis, an osteoblasts cell line MC3T3 cells was selected as the candidate of bone lining cells. We first assessed the involvement of CFTR in regulating [Cl⁻]_i by a MQAE dye in MC3T3 cells. After applying two different CFTR inhibitor, CFTR_{inh}-172 (10 μM) and glyH-101 (10 μM), the fluorescence intensity of MQAE was significantly decreased in MC3T3 cells. Compared to MLO-Y4 cells, increasement (%) of [Cl⁻]_i caused by CFTR inhibitors was similar in MC3T3 cells (Fig 3.4.1 A and B). It indicated that CFTR also contributed to mediate the Cl⁻ efflux in MC3T3 cells as MLO-Y4 cells. For the membrane potential, by using the voltage-sensitive dye DiBAC₄(3) (Bis-(1,3-Dibutylbarbituric Acid) Trimethine Oxonol), we observed similar variation for membrane hyperpolarization in MC3T3 cells after the treatment of CFTR_{inh}-172 (10 μM) in MLO-Y4 cells (Fig 3.4.1 A).

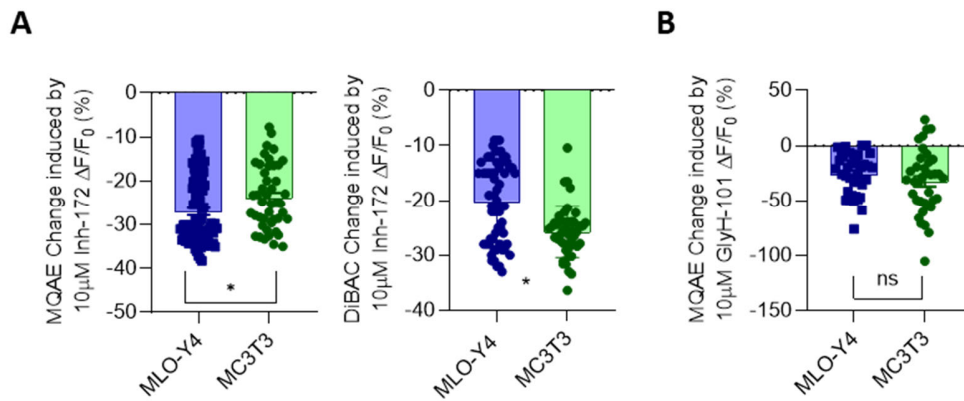


Figure 3.4.1 Effect of the CFTR inhibitors on $[Cl^-]_i$ and V_m in MLO-Y4 cells and MC3T3 cells (A) Although statically significant difference was observed in the decrement of MQAE fluorescence intensity (increment of $[Cl^-]_i$) and the decrement of DiBAC fluorescence intensity (hyperpolarization) in MLO-Y4 and MC3T3 cells after the treatment of CFTR_{inh}-172 (10 μ M), the difference is slight and inconsistent. (B) No significant difference of decrement of MQAE fluorescence intensity (increment of $[Cl^-]_i$) was found in MLO-Y4 cells and MC3T3 cells after the treatment of GlyH-101 (10 μ M). Data are mean \pm s.e.m. ns $P > 0.05$, * $P < 0.05$ by t-test.

3.4.2 pH maintenance in MC3T3 cells.

To explore the involvement of CFTR in pH regulation in MC3T3 cells, the HCO_3^-/CO_2 pulse was exerted to MC3T3 cells incubated with pH-sensitive dye BCECF by the same method used for MLO-Y4 cells. However, different from MLO-Y4 cells with an acute and dramatical intracellular acidification, the intracellular pH of MC3T3 cells resisted to be acidified but still turned to be alkalized from the original pH value. With same procedures and conditions of HCO_3^-/CO_2 pulse stimulation in MLO-Y4 cells, repeated results showed consistent resistance of MC3T3 cells towards the intracellular acidification associated with the intracellular alkalization. This

observation in MC3T3 cells under the saturated $\text{HCO}_3^-/\text{CO}_2$ suggested the distinguished role of osteoblasts and osteocytes in pH regulation of their microenvironment.

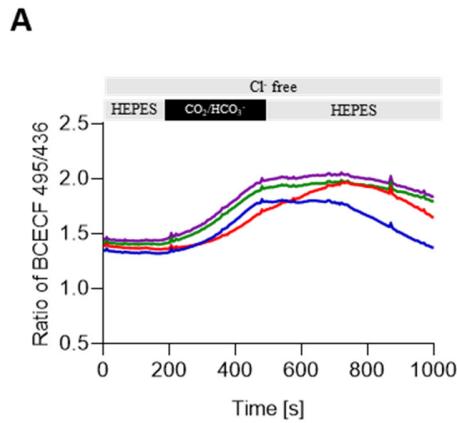


Figure 3.4.2 pH maintenance in MC3T3 cells. (A) Representative curves of intracellular pH (Ratio of BCECF, 495nm/436nm) for MC3T3 cells. After replacing the bath solution with HEPES buffer by solution perfused with saturated CO_2 gas, ratio of BCECF was sustained and associated with the increasing trend (alkalization). After changing the bath solution back to HEPES buffered solution, ratio of BCECF was slowly decreased.

3.4.3 Summary

By using fluorometric method, CFTR showed similar contributions in mediating Cl^- efflux in MC3T3 cells compared to MLO-Y4 cells. Under the saturated $\text{HCO}_3^-/\text{CO}_2$, MC3T3 cells demonstrated a different pH curve with resistance for intracellular acidification, which indicated the different role of MC3T3 and MLO-Y4 cells in regulating pH. Separating BECF and ECF, bone lining cells function as an epithelial membrane while osteocytes are immersed in BECF. It might be reasonable for MC3T3 cells demonstrated the obtuse sensitivity of saturated $\text{HCO}_3^-/\text{CO}_2$.

Chapter 4. Discussion

In summary, the present results have demonstrated previously undefined $\text{Cl}^-/\text{HCO}_3^-$ channel function of CFTR in bone cells and suggested its regulatory roles in maintaining the homeostasis of the microenvironment such as mediating electrolyte/water transport, adjusting pH and responding to mechanical stimulation.

4.1 Cl^- in the microenvironment for bone cells.

Though limited studies have done on bone cell microenvironment, Cl^- transporters in bone cells have been noted to participate in mineralization for bone matrix formation. It was reported that chloride proton exchangers genes *CLC3* and *CLC5* were highly expressed in mouse and human osteoblasts (Blair et al., 2017). Double knockout of the two genes resulted in defective osteoblast mineralization *in vitro* (Larrouture et al., 2015). The present electrophysiological and fluorometric imaging results demonstrated the channel function of CFTR in mediating Cl^- efflux in MLO-Y4 cells *in vitro*. The bath solution that we used in the experiments (both patch-clamp and imaging) contained about 142 mM Cl^- , which was higher than 130 mM, the Cl^- concentration of BECF in cortical veal bone as indirectly measured by an early study (Neuman & homeostasis, 1971, as cited in Green & Kleeman, 1991). Therefore, it is likely that osteocytes have a high intracellular Cl^- concentration (higher than 142 mM) and CFTR may mediate Cl^- efflux in the physiological situation *in vivo* too, contributing to the Cl^- homeostasis in bone cell microenvironment. However, several questions remain such as whether CFTR-mediated Cl^- efflux could directly participate in calcium or phosphate deposit for mineralization, or indirectly through regulation of Cl^- transporters/channels. In addition to mineralization, would CFTR-mediated Cl^- efflux be important to other activities of bone cells such as volume change and cell migration as noted in other cell

types? Further investigation into these possible roles of CFTR in bone cells in future will be needed to answer these questions.

4.2 pH of the microenvironment for bone cells.

Several lines of experimental evidence from the present study suggested the involvement of CFTR in regulating pH microenvironment of bone cells. First, CFTR was found to contribute to HCO_3^- secretion in osteocytes, which may alter the chemical equilibrium between CO_2 , water, and H^+ in the extracellular fluid of bone cells. Second, the recovery from CO_2 -induced acidification was observed to be impaired in CFTR knockout osteocyte line. Third, genes for the H^+ pump (V-ATPase) were found to be upregulated in bone tissues of CFTR deficient mice. pH of the microenvironment surrounding bone cells is essential to both bone formation and resorption. For the mineralization accumulation, abnormal pH would damage the conversion of calcium and phosphate to hydroxyapatite for osteoblasts. For bone resorption, the acidified environment is necessary to dissolve the bone matrix. Although many researches on osteoblasts and osteoclasts for their targeted functions in the bone remodelling process, evidence pointed out that osteocytes themselves could remove their perilacunar/canalicular matrix under different metabolic requirements by secreting H^+ . The direct role of osteocytes in secreting H^+ is believed to be responsible for the acute Ca^{2+} mobilization in bone tissues to meet the instantaneous requirement of Ca^{2+} homeostasis in blood. Such osteocytic osteolysis was recently demonstrated. Parathyroid hormone-related protein (PTHrP) can activate molecular components in osteocytes, which are known to be utilized by osteoclasts during bone remodelling (Qing et al., 2012). Among those molecules, the increased H^+ secretion was achieved by enhancing the expression of vacuolar-ATPase, an ATP-driven proton pump in osteocytes, which acidified their fluidic milieu to mobilize Ca^{2+} . Another study on lactating mice showed that osteocytes demonstrated the ability to acidify

their microenvironment via ATP6V0D2 (a subunit of V-ATPase) (Jähn, Kelkar, Zhao, Xie, Tiede-Lewis, Dusevich, Dallas, & Bonewald, 2017). Given such increasingly realized importance of osteocytes in pH regulation in bone remodeling and mineral homeostasis, the presently demonstrated association of CFTR with pH regulators (HCO_3^- , V-ATPase etc.) in osteocyte may provide new insights into osteocyte physiology as well as pathophysiology associated with CFTR deficiency. Nevertheless, how exactly CFTR regulates pH in osteocytes remains unclear. It should be noted that in other cell types, CFTR were widely reported to be associated with many H^+ -related channels or transporters, such as Na^+/H^+ exchanger (NHE) and proton-gated Na^+ channels (ASIC) (Benharouga et al., 2003; Guerra et al., 2005; Su et al., 2006), as well as V-ATPase (A. M. Collaco, Geibel, Lee, Geibel, & Ameen, 2013), either through protein-protein interactions or unclear mechanisms. Direct or indirect roles of CFTR in bone cells will need to be further studied.

As one type of water-soluble hormone, PTHrP could increase the concentration of intracellular cAMP in epithelial cells (Ferrari et al., 1993). It suggested that CFTR could also be activated by the treatment of PTHrP, as the primary gating stimulus of CFTR (Protein kinase A) was activated by cAMP.

4.3 Environmental cues for bone cells.

Bone cells including osteocytes are known to be subject to the regulation by their environmental cues including hormones, neurotransmitters, paracrine factors and physical/mechanical stimulations. It is important to note that CFTR channel function in osteocytes is presently demonstrated to be clearly activated by forskolin, a reagent to stimulate cAMP elevation. Physiologically, many environmental factors are known to alter bone activities through their receptors' activation of cAMP-dependent pathways in bone cells (e.g. calcitonin, glucagon,

Thyroid-stimulating hormone, and PTHrP). It therefore suggests the critical involvement of CFTR in the dynamic activities of bone cells under different physiological conditions. Interestingly, CFTR's sensitivity to glucose has been reported in insulin-secreting pancreatic islet beta cells (Guo et al., 2014). Environment glucose levels are key to bone cell metabolism and function. A recent study showed that elevated glucose directly acts on osteocytes to upregulate sclerostin expression (Pacicca et al., 2019). The glucose-sensitivity of CFTR in bone cells can be studied in future.

Moreover, the present study showed possible involvement of CFTR in mechanosensitivity of osteocytes. However, the present evidence is still very limited and many questions are unanswered regarding CFTR and osteocyte mechano-sensitivity. Direct patch-clamp measurement of CFTR sensitivity to mechanical forces in osteocytes will be needed. Specific animal models (e.g. tail suspension) to study mechanical forces upon bones in conjunction of CFTR-deficiency models will be required to understand whether and how CFTR really contributes to mechano-stimulated bone formation or remodelling. Other key questions are also presented: what type of mechanical forces can modulate CFTR in osteocytes? Would CFTR be important for physiotherapy of bone disorders? Further studies are therefore awaited.

4.4 Conclusion remarks

Although more and more studies on bone physiology have shifted the focus onto osteocytes, less attention has been paid to how the interaction between the microenvironment and osteocytes. The present study is the first, to the best of our knowledge, to show the channel function of CFTR for interacting with microenvironment of osteocytes and its physiological involvements in osteocytes for maintaining bone health. It could improve our understanding of CFTR as the pathogenetic factor under Cystic fibrosis bone disease (CFBD). Besides, the focus on ions

regulation in osteocytes may reveal more clues further the comprehension of the niche of osteocytes and contribute to tissue engineering for bone regenerative medicine.

References

- Aarden, E. M., Nijweide, P. J., & Burger, E. H. (1994). Function of osteocytes in bone. *Journal of cellular biochemistry*, 55(3), 287-299.
- Albert, B., Johnson, A., Lewis, J., Laff, M., Roberts, K., & Walter, P. J. G. S. N. Y. (2008). *Molecular Biology of the Cell*, ed. 684-686.
- Aris, R., Merkel, P., & Bachrach, L. (2005). Consensus statement: guide to bone health and disease in CF. *J Clin Endocrinol Metab*, 90, 1.888-881.896.
- Armstrong, W., Singer, L. J. C. O., & Research®, R. (1965). Composition and constitution of the mineral phase of bone. 38, 179-192.
- Arnett, T. (2003). Regulation of bone cell function by acid–base balance. *Proceedings of the Nutrition Society*, 62(2), 511-520.
- Benharouga, M., Sharma, M., So, J., Haardt, M., Drzymala, L., Popov, M., . . . Lukacs, G. L. J. J. o. B. C. (2003). The role of the C terminus and Na⁺/H⁺ exchanger regulatory factor in the functional expression of cystic fibrosis transmembrane conductance regulator in nonpolarized cells and epithelia. 278(24), 22079-22089.
- Borgens, R. B. (1984). Endogenous ionic currents traverse intact and damaged bone. *Science*, 225(4661), 478-482.
- Bozal, C. B., Sánchez, L. M., & Ubios, Á. M. J. A. O. L. (2012). The lacuno-canalicular system (LCS) and osteocyte network of alveolar bone by confocal laser scanning microscopy (CLSM). 25(1), 122-129.
- Bronckers, A., Kalogeraki, L., Jorna, H. J., Wilke, M., Bervoets, T. J., Lyaruu, D. M., . . . de Jonge, H. J. B. (2010). The cystic fibrosis transmembrane conductance regulator (CFTR)

- is expressed in maturation stage ameloblasts, odontoblasts and bone cells. *46*(4), 1188-1196.
- Buenzli, P. R., & Sims, N. A. J. B. (2015). Quantifying the osteocyte network in the human skeleton. *75*, 144-150.
- Bushinsky, D. A., Chabala, J., Levi-Setti, R. J. A. J. o. P.-E., & Metabolism. (1989). Ion microprobe analysis of bone surface elements: effects of 1, 25 (OH) 2D3. *257*(6), E815-E822.
- Busse, J. W., Bhandari, M., Kulkarni, A. V., & Tunks, E. (2002). The effect of low-intensity pulsed ultrasound therapy on time to fracture healing: a meta-analysis. *Cmaj*, *166*(4), 437-441.
- Castellani, S., Guerra, L., Favia, M., Di Gioia, S., Casavola, V., & Conese, M. (2012). NHERF1 and CFTR restore tight junction organisation and function in cystic fibrosis airway epithelial cells: role of ezrin and the RhoA/ROCK pathway. *Laboratory investigation*, *92*(11), 1527.
- Chen, J.-H., Liu, C., You, L., & Simmons, C. A. J. J. o. b. (2010). Boning up on Wolff's Law: mechanical regulation of the cells that make and maintain bone. *43*(1), 108-118.
- Coakley, R. D., Grubb, B. R., Paradiso, A. M., Gatzky, J. T., Johnson, L. G., Kreda, S. M., . . . Boucher, R. C. (2003). Abnormal surface liquid pH regulation by cultured cystic fibrosis bronchial epithelium. *Proceedings of the National Academy of Sciences*, *100*(26), 16083-16088.
- Collaco, A., Geibel, P. J., Geibel, J. P., & Ameen, N. (2011). CFTR is Necessary for Vacuolar ATPase Proton Pump (VATPase) Localization and Function in Polarized Intestinal CaCo2BBE Cells. *Gastroenterology*, *140*(5), S-645.

- Collaco, A. M., Geibel, P., Lee, B. S., Geibel, J. P., & Ameen, N. A. (2013). Functional vacuolar ATPase (V-ATPase) proton pumps traffic to the enterocyte brush border membrane and require CFTR. *American Journal of Physiology-Cell Physiology*, *305*(9), C981-C996.
- Cowin, S. C., & Cardoso, L. (2015). Blood and interstitial flow in the hierarchical pore space architecture of bone tissue. *Journal of biomechanics*, *48*(5), 842-854.
- Cvetkovic, V., Najman, S., Rajkovic, J., Zabar, A., Vasiljevic, P., Djordjevic, L. B., & Trajanovic, M. J. V. M. (2013). A comparison of the microarchitecture of lower limb long bones between some animal models and humans: a review. *58*(7).
- Dallas, S. L., Prideaux, M., & Bonewald, L. F. (2013). The osteocyte: an endocrine cell... and more. *Endocrine reviews*, *34*(5), 658-690.
- Ferrari, S., Rizzoli, R., Chaponnier, C., Gabbiani, G., Bonjour, J.-P. J. A. J. o. P.-E., & Metabolism. (1993). Parathyroid hormone-related protein increases cAMP production in mammary epithelial cells. *264*(3), E471-E475.
- Florencio-Silva, R., Sasso, G. R. d. S., Sasso-Cerri, E., Simões, M. J., & Cerri, P. S. (2015). Biology of bone tissue: structure, function, and factors that influence bone cells. *BioMed research international*, *2015*.
- Green, J., & Kleeman, C. R. J. C.-R. H. I. (1991). The role of bone in the regulation of systemic acid-base balance. *91*, 61-76.
- Guerra, L., Fanelli, T., Favia, M., Riccardi, S. M., Busco, G., Cardone, R. A., . . . Conese, M. J. J. o. B. C. (2005). Na⁺/H⁺ exchanger regulatory factor isoform 1 overexpression modulates cystic fibrosis transmembrane conductance regulator (CFTR) expression and activity in human airway 16HBE14o-cells and rescues ΔF508 CFTR functional expression in cystic fibrosis cells. *280*(49), 40925-40933.

- Guggino, W. B., & Stanton, B. A. (2006). Mechanisms of disease: New insights into cystic fibrosis: molecular switches that regulate CFTR. *Nature reviews Molecular cell biology*, 7(6), 426.
- Guo, J. H., Chen, H., Ruan, Y. C., Zhang, X. L., Zhang, X. H., Fok, K. L., . . . Sun, X. J. N. c. (2014). Glucose-induced electrical activities and insulin secretion in pancreatic islet β -cells are modulated by CFTR. 5(1), 1-10.
- Huang, C., & Ogawa, R. (2010). Mechanotransduction in bone repair and regeneration. *The FASEB Journal*, 24(10), 3625-3632.
- Jähn, K., Kelkar, S., Zhao, H., Xie, Y., Tiede-Lewis, L. M., Dusevich, V., . . . Bonewald, L. F. (2017). Osteocytes acidify their microenvironment in response to PTHrP in vitro and in lactating mice in vivo. *Journal of Bone and Mineral Research*, 32(8), 1761-1772.
- Jähn, K., Kelkar, S., Zhao, H., Xie, Y., Tiede-Lewis, L. M., Dusevich, V., . . . Research, M. (2017). Osteocytes acidify their microenvironment in response to PTHrP in vitro and in lactating mice in vivo. 32(8), 1761-1772.
- Javier, R.-M., & Jacquot, J. (2011). Bone disease in cystic fibrosis: what's new? *Joint Bone Spine*, 78(5), 445-450.
- Kovacs, C. S. (2014). Bone development and mineral homeostasis in the fetus and neonate: roles of the calciotropic and phosphotropic hormones. *Physiological Reviews*, 94(4), 1143-1218.
- Le Henaff, C., Mansouri, R., Modrowski, D., Zarka, M., Geoffroy, V., Marty, C., . . . Marie, P. J. (2015). Increased NF- κ B activity and decreased Wnt/ β -catenin signaling mediate reduced osteoblast differentiation and function in Δ F508 cystic fibrosis transmembrane

- conductance regulator (CFTR) mice. *Journal of Biological Chemistry*, 290(29), 18009-18017.
- Leighton, R., Watson, J. T., Giannoudis, P., Papakostidis, C., Harrison, A., & Steen, R. G. J. I. (2017). Healing of fracture nonunions treated with low-intensity pulsed ultrasound (LIPUS): a systematic review and meta-analysis. *48(7)*, 1339-1347.
- Lou, S., Lv, H., Li, Z., Zhang, L., & Tang, P. (2017). The effects of low-intensity pulsed ultrasound on fresh fracture: A meta-analysis. *Medicine*, 96(39).
- Malhan, D., Muelke, M., Rosch, S., Schaefer, A. B., Merboth, F., Weisweiler, D., . . . El Khassawna, T. J. F. i. e. (2018). An optimized approach to perform bone histomorphometry. *9*, 666.
- Marenzana, M., Shipley, A., Squitiero, P., Kunkel, J., & Rubinacci, A. (2005). Bone as an ion exchange organ: evidence for instantaneous cell-dependent calcium efflux from bone not due to resorption. *Bone*, 37(4), 545-554.
- Miller, S. C., Bowman, B., & Jee, W. (1989). Bone lining cells: structure and function. *Scanning microscopy*, 3(3), 953-960; discussion 960-951.
- Moran, O. J. C., & Sciences, M. L. (2017). The gating of the CFTR channel. *74(1)*, 85-92.
- Pacicca, D. M., Brown, T., Watkins, D., Kover, K., Yan, Y., Prideaux, M., & Bonewald, L. J. S. r. (2019). Elevated glucose acts directly on osteocytes to increase sclerostin expression in diabetes. *9(1)*, 1-11.
- Park, H. W., Nam, J. H., Kim, J. Y., Namkung, W., Yoon, J. S., Lee, J. S., . . . Kim, K. H. J. G. (2010). Dynamic regulation of CFTR bicarbonate permeability by [Cl⁻]_i and its role in pancreatic bicarbonate secretion. *139(2)*, 620-631.

- Perez-Vilar, J., Olsen, J. C., Chua, M., & Boucher, R. C. (2005). pH-dependent intraluminal organization of mucin granules in live human mucous/goblet cells. *Journal of Biological Chemistry*, 280(17), 16868-16881.
- Qing, H., Ardeshirpour, L., Divieti Pajevic, P., Dusevich, V., Jähn, K., Kato, S., . . . research, m. (2012). Demonstration of osteocytic perilacunar/canalicular remodeling in mice during lactation. 27(5), 1018-1029.
- Quinton, P. M. (2007). Cystic fibrosis: lessons from the sweat gland. *Physiology*, 22(3), 212-225.
- Reddy, M., & Quinton, P. (1989). Localization of Cl-conductance in normal and Cl-impermeability in cystic fibrosis sweat duct epithelium. *American Journal of Physiology-Cell Physiology*, 257(4), C727-C735.
- Rho, J.-Y., Kuhn-Spearing, L., Zioupos, P. J. M. e., & physics. (1998). Mechanical properties and the hierarchical structure of bone. 20(2), 92-102.
- Riddle, R. C., & Donahue, H. J. J. J. o. o. r. (2009). From streaming-potentials to shear stress: 25 years of bone cell mechanotransduction. 27(2), 143-149.
- Rocheftort, G. Y., Pallu, S., & Benhamou, C.-L. J. O. i. (2010). Osteocyte: the unrecognized side of bone tissue. 21(9), 1457-1469.
- Rubinacci, A., Benelli, F. D., Borgo, E., & Villa, I. (2000). Bone as an ion exchange system: evidence for a pump-leak mechanism devoted to the maintenance of high bone K⁺. *American Journal of Physiology-Endocrinology And Metabolism*, 278(1), E15-E24.
- Rubinacci, A., Covini, M., Bisogni, C., Villa, I., Galli, M., Palumbo, C., . . . Metabolism. (2002). Bone as an ion exchange system: evidence for a link between mechanotransduction and metabolic needs. 282(4), E851-E864.

- Rubinacci, A., Villa, I., Benelli, F. D., Borgo, E., Ferretti, M., Palumbo, C., & Marotti, G. J. C. t. i. (1998). Osteocyte-bone lining cell system at the origin of steady ionic current in damaged amphibian bone. *63*(4), 331-339.
- Saint-Criq, V., & Gray, M. A. (2017). Role of CFTR in epithelial physiology. *Cellular and Molecular Life Sciences*, *74*(1), 93-115.
- Shed, E. F., Haworth, C. S., Condliffe, A. M., McKeon, D. J., Scott, M. A., & Compston, J. E. J. T. (2007). Cystic fibrosis transmembrane conductance regulator (CFTR) is expressed in human bone. *62*(7), 650-651.
- Stalvey, M. S., Clines, K. L., Havasi, V., McKibbin, C. R., Dunn, L. K., Chung, W. J., & Clines, G. A. J. P. O. (2013). Osteoblast CFTR inactivation reduces differentiation and osteoprotegerin expression in a mouse model of cystic fibrosis-related bone disease. *8*(11), e80098.
- Su, X., Li, Q., Shrestha, K., Cormet-Boyaka, E., Chen, L., Smith, P. R., . . . Ji, H.-L. J. J. o. B. C. (2006). Interregulation of proton-gated Na⁺ channel 3 and cystic fibrosis transmembrane conductance regulator. *281*(48), 36960-36968.
- Wongdee, K., Pandaranandaka, J., Teerapornpantakit, J., Tudpor, K., Thongbunchoo, J., Thongon, N., . . . Charoenphandhu, N. (2008). Osteoblasts express claudins and tight junction-associated proteins. *Histochemistry and cell biology*, *130*(1), 79-90.
- Wysolmerski, J. J. J. B. r. (2012). Osteocytic osteolysis: time for a second look? , *1*.
- Yavropoulou, M., Yovos, J. J. J. o. m., & interactions, n. (2016). The molecular basis of bone mechanotransduction. *16*(3), 221.

- Yu, B., Pacureanu, A., Olivier, C., Cloetens, P., & Peyrin, F. J. S. r. (2020). Assessment of the human bone lacuno-canalicular network at the nanoscale and impact of spatial resolution. *10*(1), 1-12.
- Zhang, W. K., Wang, D., Duan, Y., Loy, M. M., Chan, H. C., & Huang, P. J. N. c. b. (2010). Mechanosensitive gating of CFTR. *12*(5), 507-512.